DETERMINATION OF PHOTON MOMENTUM TRANSFER BETWEEN
DIFFERENT MEDIUMS USING INTERFEROMETRY OF AN ANGLED SILICA
FIBER FILAMENT

A THESIS SUBMITTED TO
THE GRADUATE SCHOOL OF NATURAL AND APPLIED SCIENCES
OF
MIDDLE EAST TECHNICAL UNIVERSITY

BY

EKİN ÖZGÖNÜL

IN PARTIAL FULFILLMENT OF THE REQUIREMENTS
FOR
THE DEGREE OF MASTER OF SCIENCE
IN
PHYSICS

AUGUST 2016

Approval of the thesis:

DETERMINATION OF PHOTON MOMENTUM TRANSFER BETWEEN DIFFERENT MEDIUMS USING INTEREFEROMETRY OF AN ANGLED SILICA FIBER FILAMENT

submitted by **EKİN ÖZGÖNÜL** in partial fulfillment of the requirements for the degree of **Master of Science in Physics Department, Middle East Technical University** by,

Prof. Dr. Gülbin Dural Ünver   _____
Dean, Graduate School of **Natural and Applied Sciences**

Prof. Dr. Sadi Turgut   _____
Head of Department, **Physics Department**

Prof. Dr. Ahmet Oral   _____
Supervisor, **Physics Department, METU**

Examining Committee Members:

Prof. Dr. Oğuz Gülseren   _____
Physics Department, Bilkent University

Prof. Dr. Ahmet Oral   _____
Supervisor, **Physics Department, METU**

Doç. Dr. Alpan Bek   _____
Physics Department, METU

Prof. Dr. Raşit Turan   _____
Physics Department, METU

Doç.Dr. Mehmet Z. Baykara   _____
Mechanical Engineering Department, Bilkent University

                                             Date: 07.09.2016

I hereby declare that all information in this document has been obtained and presented in accordance with academic rules and ethical conduct. I also declare that, as required by these rules and conduct, I have fully cited and referenced all material and results that are not original to this work.

Name, Last name: Ekin Özgönül

Signature   :

ABSTRACT

DETERMINATION OF PHOTON MOMENTUM TRANSFER BETWEEN DIFFERENT MEDIUMS USING INTEREFEROMETRY OF AN ANGLED SILICA FIBER FILAMENT

Özgönül, Ekin
M.S., Department of Physics
Supervisor   : Prof. Dr. Ahmet Oral

August 2016, 52 pages

There is a long standing dilemma about the value of photon momentum in dielectric media. Two rivaling views differ on both the magnitude and the direction of momentum but both are seemingly sound from a theoretical standpoint. Experimental work done also has evidence favoring both Abraham and Minkowski theories with different experiments supporting one of them. Aim of this thesis is to measure the deflection of a silica fiber filament with an angled end face and measure the displacement resulting from the momentum transfer between the fiber and air interface. The results found are within the error margins predicted by the Minkowski theory. Since the error margins are relatively large, the results are not conclusive enough to disprove the Abraham theory, however they are in strong favor of the Minkowski theory.

Keywords: Abraham-Minkowski, Photon Momentum

ÖZ

FARKLI ORTAMLAR ARASI GEÇİŞ SIRASINDA FOTON MOMENTUM DEĞİŞİMİNİN AÇILI CAM FİBER ELYAFI ÜZERİNDEN İNTERFEROMETRİK ÖLÇÜMÜ

Özgönül, Ekin
Master, Fizik Bölümü
Tez Yöneticisi   : Prof. Dr. Ahmet Oral

Ağustos 2016, 52 sayfa

Uzunca bir süredir dielektrik malzemeler içerisindeki ışık momentumunun değeri hakkında çözülememiş bir ikilem bulunmaktadır. İki karşı görüş momentumun hem büyüklüğü hem de yönü hakkında farklı görüşler sunmakta, fakat teorik altyapı olarak ikisinin de temelleri sağlam gözükmektedir. Yapılan deneysel araştırmalarda ise hem Abraham hem de Minkowski teorilerini destekleyen sonuçlar ortaya çıkmıştır. Bu tezin amacı ucuna açı verilmiş cam fiber elyafı kullanarak yüzeydeki momentum değişimi sonucu ortaya çıkan salınım genliğinin interferometre kullanılarak ölçülmesidir. Elde edilen sonuçlar Minkowski teorisi tarafından beklenen aralığa yakın çıkmıştır. Hata payları geniş olduğundan dolayı Abraham teorisini elemek için yeterli bağıntı olmasa da sonuçlar Minkowski teorisini destekler şekildedir.

Anahtar Kelimeler: Abraham-Minkowski, Işık Momentumu

ACKNOWLEDGMENTS

I'd like to thank my advisor Prof. Dr. Ahmet Oral for introducing me to such an exciting subject and his constant help throughout the years. Without him, we would not be able to establish the SPMG Lab from the ground up and have it working in such a short time.

I'd also like to thank my lab partners Ercan Karagöz, Uğur Yiğit İnkaya, Burak Yıldız, Shumaila Karamat and Sameena Shahzaman throughout the years for their invaluable help in both experiments and daily matters.

One of my lab partners, Yiğit Uysallı, whom I'd like to thank not only for our times spent in the lab, but also for countless hours we spent together ever since we first met at the beginning of our paths in studying physics. His and Doğa Uysallı's friendship and advice has always helped me immeasurably through the hardest of times. I am extremely lucky for having such wonderful friends.

My beloved cats, Behzat and Gölge have always been a constant source of support, even though their incessant cries for attention and endless need for petting might seem tiring, their pure sweet love more than makes up for it.

My old dorm and flat mate Kerem Hürcan Güllü has my gratitude for supporting me in daily tasks throughout the writing of this thesis.

I'd like to thank my fellow bandmates Esatcan Apak, Mehmet Karaman, Mustafa Cem Lider and Oğuz Kerem Şengöz for the wonderful hours spent making music.

My parents and siblings, who are instrumental to who I am today have my most sincere thanks for always encouraging and guiding me to pursue my dreams.

TABLE OF CONTENTS

LIST OF FIGURES

FIGURES

LIST OF ABBREVIATIONS

IR   Infrared

FPS   Frames per second

TTL   Transistor-transistor logic

PEC   Perfect electrical conductor

PMC Perfect magnetic conductor

AFM Atomic force microscopy

CHAPTER I

INTRODUCTION

The phenomena of light has always been a source of research and fascination in the scientific community throughout decades. After Maxwell proposed that light is an electromagnetic wave in his 1865 paper [1] it is clearly apparent that photons play a unique role in how the universe works. However, even though the realization that light can have such a grandiose importance might be a fundamentally basic piece of knowledge in the 21th century, there are still remaining ambiguous questions about it such as the Abraham – Minkowski Dilemma regarding photon momentum in dielectric media. The scope of the debate is particularly interesting when one also considers the fact that enquiry into photon momentum can be indirectly traced back to as early as 1619 to Kepler [2] where he put forth the concept of light imparting momentum on objects by investigating the tail of comets. This thesis aims to shed some light on the Abraham – Minkowski debate by first examining the theoretical grounds, comparing the theory with experimental results, and devising a simple setup to test some of the more controversial experimental results published recently by She et al. [3].

I.1 Photon Momentum

The property that light carries momentum was proposed as early as 1619 by Kepler [2], long before phenomenon of electricity, magnetism and light were united into the electromagnetic theory. The experimental proof for the existence of photon momentum was given by Pyotr Lebedev in 1901 [4] and by Ernest Fox Nichols and

Gordon Ferrie Hull in 1903 [5]. In vacuum, a single photon has a momentum uniquely defined by its wavelength of magnitude $\hbar\mathbf{k}$ where $\mathbf{k}$ denotes the wavevector with the property $|\mathbf{k}| = 2\pi/\lambda$. The direction of a photons linear momentum is in the same direction as the wavevector for any isotropic and homogenous media, the only requirement being that the group and phase velocities do not differ in direction.

I.2 Photon Momentum in Dielectrics

Minkowski, in his paper written in 1908 [6] has put forward the $\mathbf{D} \times \mathbf{B}$ expression for the momentum density in dielectric media. Within his formulation the following relationship can be derived by integrating the Lorentz force density over a finite closed volume and substituting the constitutive relations for the fields.

$$\frac{d}{dt}(\mathbf{p}_\mathrm{m} + \mathbf{D} \times \mathbf{B})_i = \sum_{j=1}^{3} \frac{\partial T_{ij}^M}{\partial x_j} \qquad \text{(Eq.1)}$$

Where $\mathbf{p}_m$ is the mechanic momentum density and the stress tensor T_{ij}^M has the components

$$T_{ij}^M = E_i D_j + H_i B_j - \frac{1}{2}(\mathbf{E} \cdot \mathbf{D} + \mathbf{H} \cdot \mathbf{B})\delta_{ij} \qquad \text{(Eq.2)}$$

It is easily seen that the tensor has no inherent diagonal symmetry, that is unless dictated by the constitutive relations. This has gathered some criticism and led Abraham to publish two papers in 1909 and 1910 in which he formulated the momentum density as $\frac{1}{c^2}\mathbf{E} \times \mathbf{H}$ [7,8]. For an isotropic linear medium which is nondispersive, rewriting Eq.1 to include the Abraham momentum density in explicit form is easy using the constitutive relations $\mathbf{D} = \epsilon\mathbf{E}$ & $\mathbf{B} = \mathbf{\mu H}$ together with the fact that the refractive index can be written as $n^2 = \epsilon\mu$. This will yield the relation shown in Eq.3a.

$$\frac{d}{dt}(\mathbf{p}_\mathrm{m} + \frac{1}{\mathbf{C}^2}(\mathbf{E} \times \mathbf{H})_i + (n^2 - 1)(\mathbf{E} \times \mathbf{H}))_i = \sum_{j=1}^{3} \frac{\partial T_{ij}^M}{\partial x_j} \qquad \text{(Eq.3a)}$$

or alternatively;

$$\frac{d}{dt}\left(\mathbf{p}_{\mathrm{m}} + \frac{1}{\mathbf{c}^2}(\mathbf{E} \times \mathbf{H})\right)_i = \sum_{j=1}^{3} \frac{\partial T_{ij}^A}{\partial x_j} \qquad (\text{Eq.3b})$$

In which the stress tensor T_{ij}^A has the form

$$T_{ij}^A = \frac{1}{2}\left(E_i D_j + E_j D_i\right) + \frac{1}{2}\left(H_i B_j + H_j B_i\right) - \frac{1}{2}(\mathbf{E} \cdot \mathbf{D} + \mathbf{H} \cdot \mathbf{B})\delta_{ij} \qquad (\text{Eq.4})$$

One can quickly realize that the tensor is diagonally symmetric since $T_{ij}^A = T_{ji}^A$.

Balazs published a paper in 1953 [9] describing a thought experiment in which the center of mass energy of a system is explored where light enters and exits a dielectric slab. His conclusion supports the Abraham momentum density as the correct form. However, a paper published by Wang in 2011 [10] argues that the Fizeau running water experiment [11] can be used to support the Minkowski momentum density analogous to the Balazs' argument. Padgett [12] gives an argument in favor of the Minkowski form by utilizing the uncertainty principle between position and momentum in a single-slit diffraction setup. Since both formulations had a firm foundation from a theoretical physics point of view, the only way to test either of them was in experiment.

I.3 History of the Abraham – Minkowski Controversy

Unfortunately, not only the experiments done were unsuccessful in deciding on a correct form, their differing results have complicated the debate even more. More recent papers by Barnett [13], Kemp [14] and Pfeifer [15] propose a resolution to the debate and review the existing literature. The authors seem to agree on the point that the Minkowski form represents the canonical momentum while the Abraham form is the kinetic one. With the addition of the correct medium contributions in each case, the calculations from Lorentz force and the total momentum of the system is conserved. What is mostly agreed upon by most authors involved in the debate is that

3

the actual question is not whether there is a unique correct form for the momentum density but rather how to attribute the different contributions arising from the medium, field and the momentum from other interacting systems that are in a given experiment. Keeping this in mind, the notable experiments are listed in this section.

One of the simplest and earliest way to measure the photon momentum in a dielectric medium was done by Jones in 1954 by reflecting light off a mirror submerged in a dielectric medium and measuring the total recoil of the mirror, the same experiment was also repeated in 1978 by Jones et al. yielding better accuracy [16, 17]. The corresponding results from the experiments support the Minkowski momentum.

In 1973, Ashkin et al. published a paper [18] in which the radiation pressure on a free liquid surface is measured through creating surface lenses on the liquid-air interface and measuring the lensing properties. The results back up the Minkowski form, but a paper by Gordon [19] argues that the force gradient due to the gaussian profile of light they have used might cause radial dipole forces not taken into account.

There is also a similar but more recent experiment by Cui in 2013 [20] in which they also squeeze in another layer of dielectric, namely a thin layer of decane, in between the air-liquid interface. Whereas Ashkin observed that the bulge at the interface was outwards hence supporting the Minkowski momentum, Cui's results have found the intermittent layer of decane to be actually compressed inwards rather than bulging outwards which would be predicted by the Abraham momentum.

The work of Gibson et al. [21] measures the photon drag effect in germanium and silicon in the far-infrared region. They too have results in favor of the Minkowski momentum.

Kristensen et al. published a paper in 1994 [22] in which they measured the angular momentum in dielectric media, while accepting that the linear momentum should be of the Minkowski form, their results indicate that the angular momentum happens to be independent of the refractive index n.

Walker et al.'s 1975 paper [23] meanwhile shows results that the torque amplitudes measured in a $BaTiO_3$ ceramic are correctly predicted by the Abraham form.

A more recent paper by She et al. [3] claims to measure a push force on a silica fiber for outgoing light, which is the predicted result from the Abraham form, however this work has gathered some criticism by Brevik [24] and Mansuripur [25] the former arguing that what She measured is simply the Abraham-Minkowski force density defined by $\mathbf{f}^{AM} = -(\epsilon_0/2)E^2 \nabla n^2$, not the actual electromagnetic momentum proposed by the Abraham form while the latter comments on the fact that they used the phase index n_p instead of the group index n_g in their calculations. The specified value given in She's paper is calculated using the Sellmeier Formula. Mansuripur et al. also published a paper in 2009 [26] showing numerical calculations stemming from the Lorentz force density and has argued that the calculations indicate a total pull force on the end face of a fiber rather than the push force observed by She if the mechanical momentum $\mathbf{p}_m$ is also taken correctly into account. Mansuripur et al. also notes that they are not arguing in favor of the either forms in the mentioned paper and also state that similar force measurements done on fibers might yield an insight into the nature of the problem. Also a recent comment on Mansuripur et al.'s paper by Torchigin et al. [28] argues that the theoretical framework used for calculations in both Mansuripur and She's papers are erroneous.

Last but not least, in a very recent paper published in 2016 by Choi et al. [28] they were able to measure the force resulting from Abraham density form in a liquid-filled hollow optical fiber. They do not seem to be proponents of either form since they claim that the force they measured does not necessarily fix the form of the momentum density however it should be noted that among the proposed resolution of dividing the forms into canonical and kinetic momentum, some authors are skeptical whether the Abraham force is actually observable, or if so, that very specific conditions might be required for measurement [14, 15].

I.4 Theoretical Analysis

In this section, arguments with theoretical basis for both forms are analyzed and compared. First argument would be the Balazs' thought experiment [9], sometimes referred to as the "Einstein box" thought experiment, which supports Abraham momentum as the correct momentum. Following Balazs' original argument, let us

assume that a photon is travelling in the same direction as the long end of a dielectric slab shown in Figure 1.
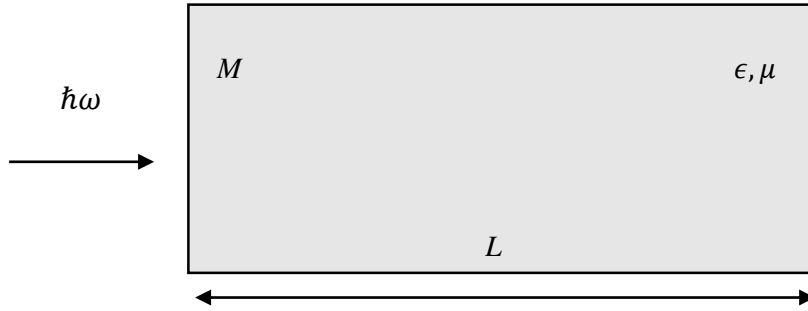

Figure 1: Pictorial representation of the "Einstein box" thought experiment

Outside the slab, the photon has an equivalent mass of $m = E/c^2$. Let $t = 0$ denote the moment that light enters the slab and $t = \tau$ denote the moment that light exits the slab. There are a few assumptions that has to be made which are as follows:

(a) The mass M of the slab is much bigger than the equivalent mass attributed to the photon; $M \gg m$. This is to ensure that the velocity and therefore the kinetic energy of the slab to be negligible during the analysis

(b) The wavelength of the incoming light λ is much smaller than the long end of the dielectric; $\lambda \ll L$

(c) There are no reflections at the boundaries

Balazs solves the problem first by evaluating the displacement of center of mass-energy, and then looking at three different cases in which there would be no reflections at the boundaries. For the first case he assumes the angle of incidence of the incoming light to be Brewster's angle. In the second case he assumes that the light strikes the slab in the same direction as the surface normal and setting $\epsilon = \mu$. Finally he assumes that $\epsilon \,\&\, \mu$ to vary slowly with respect to the direction of propagation so that any reflection will be negligible. Justification for the validity of the third assumption will not be discussed here, however the results obtained from his center of mass-energy argument is quickly summarized below:

At $t = \tau$, the distance traveled by the light will be $R_2 = v_2\tau$, where v_2 denotes the velocity inside the slab. If there was no slab, the distance travelled would be $R_1 = c\tau$. Supposing that the slab did not move during $0 < t < \tau$, the center of mass should have moved an amount of $\frac{m}{(m+M)}(c - v_2)\tau$, correspondingly, the displacement from the slab gives the contribution $\frac{M}{(m+M)}\xi$, thus equating two expressions will give us $M\xi = m(c - v_2)\tau$. Thus the slab has the momentum $m(c - v_2)$. From the conservation of momentum we have Eq.5a

$$mc - \frac{M\xi}{\tau} = mv_2 \qquad\qquad\qquad \text{(Eq.5a)}$$

$$\frac{M\xi}{\tau} = mc\left(1 - \frac{1}{n}\right) \qquad\qquad\qquad \text{(Eq.5b)}$$

Where we employed the fact that $v_2 = \frac{c}{n}$. For a relativistic treatment, please refer to the 2011 paper by Ramos [29]. It is worthwhile to note Padgett's paper [12], in which he reformulates the Einstein box thought experiment without a need for a medium instead using two mirrors as a delay line. The illustration is shown in Figure 2.

The argument given is that the use of the Minkowski momentum would be improper in deciding the movement of the block since it itself contains the mechanical momentum of the medium.

The second argument, which supports the Minkowski momentum is diffraction from a single slit. The simple analysis given by Padgett in the same paper is outlined below:

Let Δx be the width of the slit, the first diffraction minimum can be approximated as $\theta = \lambda/\Delta x$ since it will lie in the region where the small angle approximation holds. $\Delta\theta$ for the zero-order maximum is given by $\Delta\theta \approx 2\Delta p_x/p_0$ for small diffraction angles. Using the uncertainty principle for position and momentum in the slits direction; $\Delta x\Delta p_x \geq \frac{\hbar}{2}$ we have Eq.6.
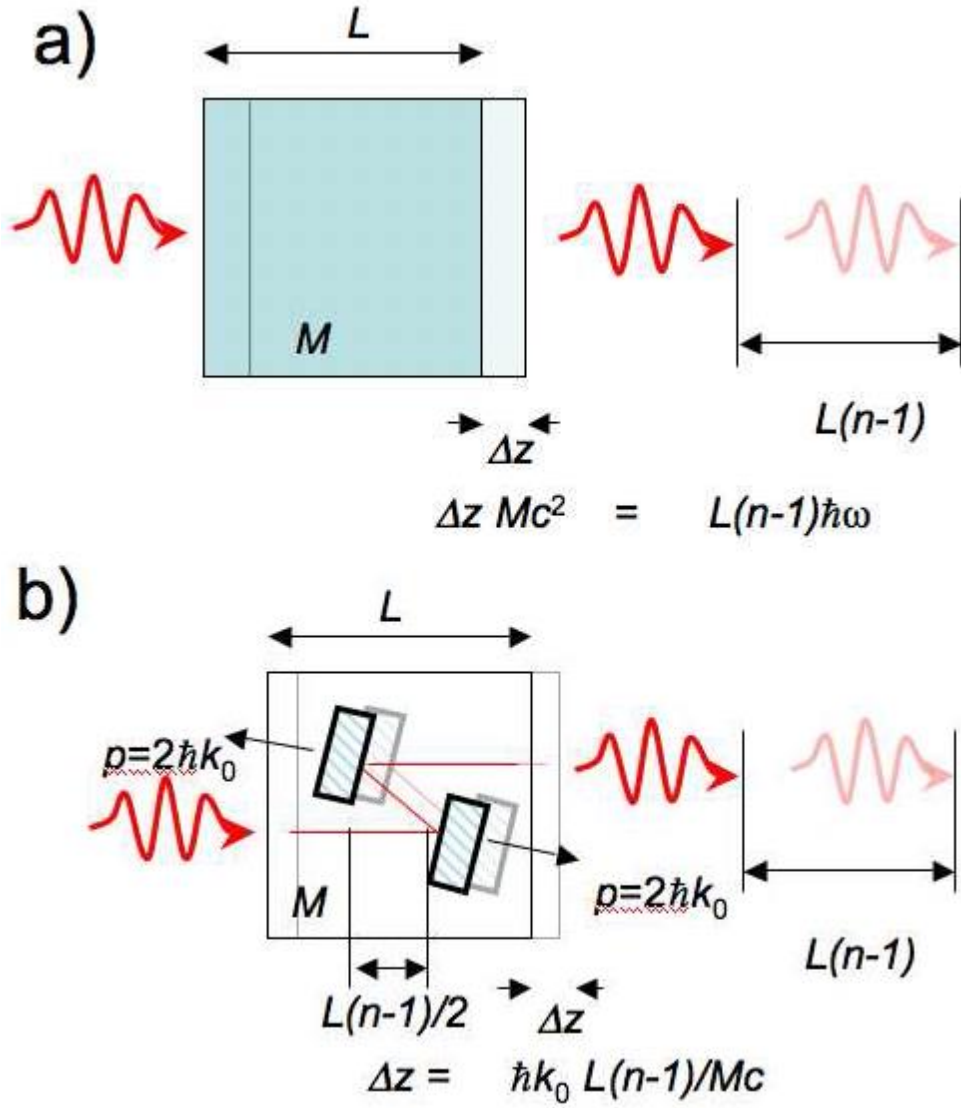
Figure 2: Illustration of the modified "Einstein box" thought experiment [12]

$$\Delta\theta = {}^{2\hbar}/_{\Delta x p_0} \qquad \text{(Eq.6)}$$

If we consider the case wherein the space consisted of a medium with refractive index n, the wavelength inside would reduce to $\frac{\lambda}{n}$ thus the angular spread would also be reduced by the same factor. Since the physical dimensions of the slit remain as it is when inside another medium, the change can only be attributed to the p_0 term hence inside a dielectric medium, the momentum of light should be np_0 supporting the Minkowski form.

8

I.5 Experimental Evidence

As stated previously, the experimental evidence for the correctness of two forms is also divided in regards that each has experimental evidence in favor of them.

One of the first experiments done to resolve the conflict was that of Jones' [16], which he later repeated in 1978 to a better accuracy [17]. The experimental setup basically consists of a mirror attached to a torsion balance, inside a container which can be filled with various fluids. The mirrors are illuminated from a light source outside the container. The diagram of the setup is given in Figure 3 with the original captions. The light source strikes the vane, V and the measurements are taken from the mirror M wherein deflection measurements are made utilizing an optical lever amplifier. An optical lever amplifier is based on a simple idea; the mirror in its unmoved state, reflects incoming light into two photodetectors. Small angular displacements of the mirror will cause more light to shine on one of the photodetectors thus the difference between photodetector readings can be used to determine the displacement that caused the mirror to rotate. For those interested, design and analysis of such a system is given by Jones himself in a 1951 paper [30], it is presumably the same system he used in the experiment. The light source utilized for the experiment was a $12\,V, 48\,W$ Osram double-coiled tungsten filament projection lamp, run at $9.8\,V, 30\,W$ from a stabilized AC power supply. The whole optical lever amplifier is run with a negative-feedback loop to quicken the response time of the system especially when liquids are present. Observed pressure ratios agree with the values given by the Minkowski form within 1.2% accuracy. They repeated the same experiment again in 1978 [17] this time using a $632.8\,nm$ He-Ne laser and improvements to the setup in order to reduce possible errors. Averaged over seven liquids, they report that the distribution of the differences between the observed and the Minkowski value was $-(0.003\% \pm 0.053\%)$. Which amounts to an accuracy of $\approx 0.05\%$. Another experiment backing the Minkowski form is Ashkin et al.'s 1973 paper [18] where they utilized surface lensing effects to measure the force on a liquid-air interface. The experimental setup can be seen in Figure 4.
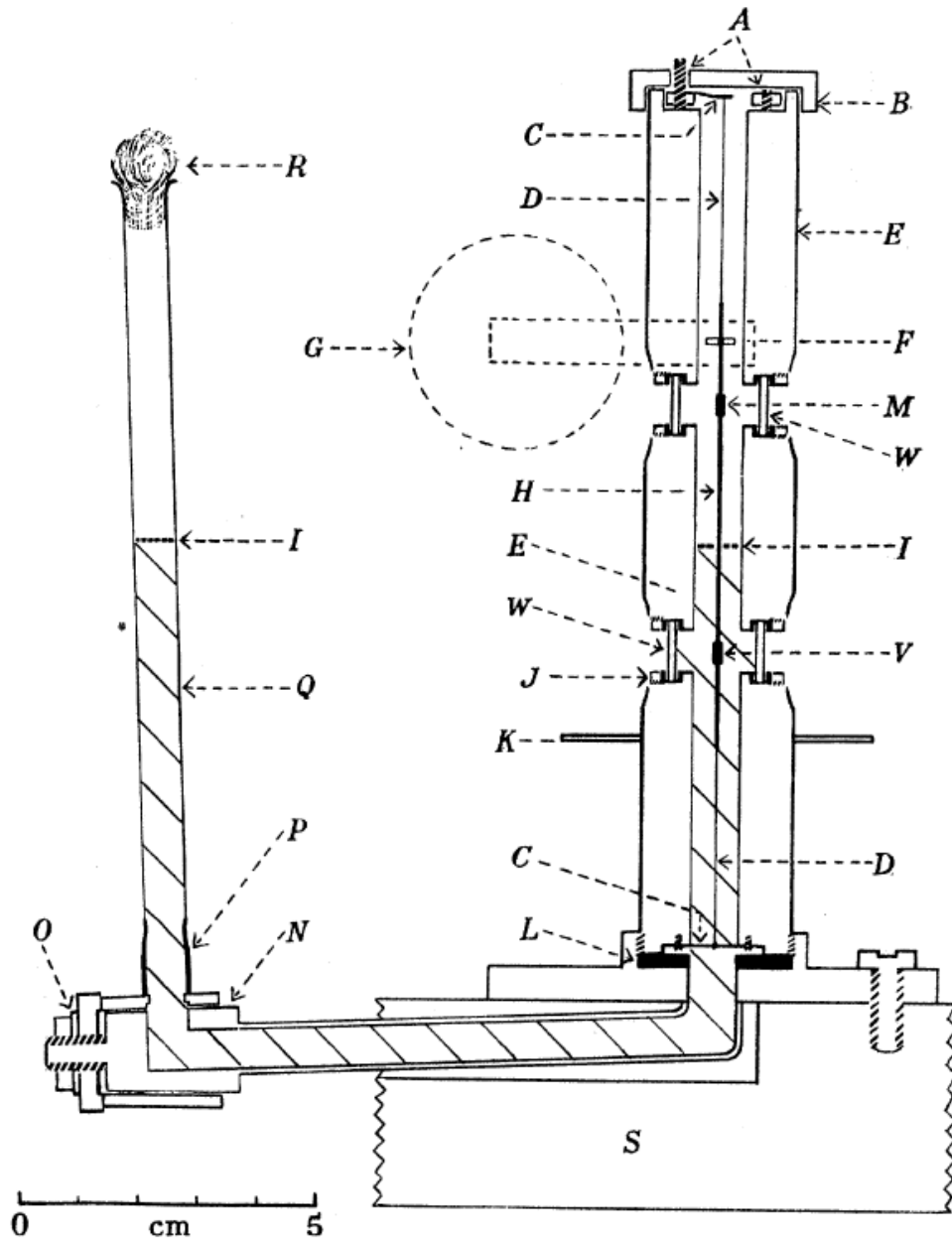
Figure 3: The suspension and its container. *A,* screws to tauten suspension; *B* brass draft cover; *C*, phosphor bronze strip 0.005 cm thick; *D*, Johnson Matthey gold alloy suspension 0.005×0.0005 cm; *E,* brass tube 0.8 cm internal diam.; *F,* magnet 0.2 cm long, 0.03 cm diam.; *G*, electromagnet; *H* 48 $s.w.g.$ copper wire; *I*, liquid levels; *J*, screwed brass ring and lead washers; *K*, support for mirrors; *L*, lead washer; *M*, silvered glass mirror $0.2 \times 0.5 \times 0.02$ cm; *N*, brass swivel joint; *O*, brass nut and washers; *P*, copper/glass seal; *G*, glass tube; *R*, cotton-wool plug; *S*, triangular cast-iron base; *V* rhodium-plated silver vane $0.2 \times 0.5 \times 0.01$ cm; *W*, circular glass windows 0.1 cm thick [16].
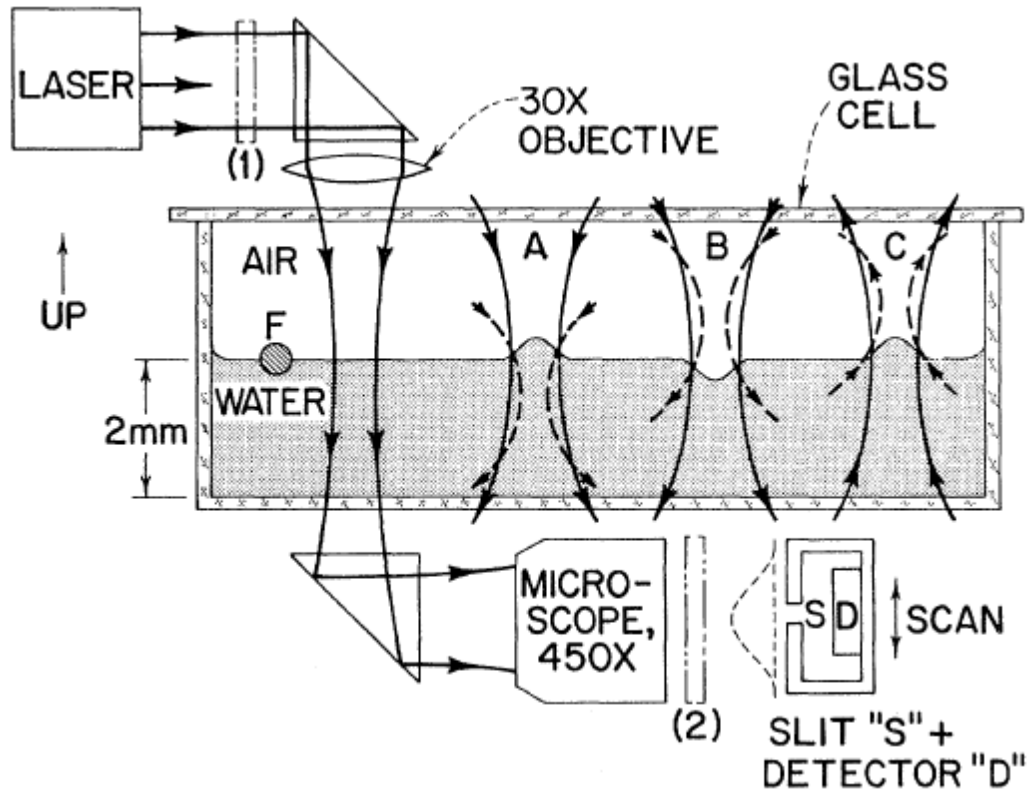
Figure 4: Basic apparatus: *A*, Beam shapes for low power (solid curve) and high power (dashed curve) for positive surface lens; *B*, shapes (for low and high power) for a negative surface lens. For *A* and *B* the beam is incident from above. *C*, beam shapes for low and high power for a positive surface lens with the beam incident from below [18].

The light source used for illumination was a $532\,nm$ Nd:YAG laser pulsing at $20\,Hz$ with a peak power of $1-4\,kW$. Their observed results agree with the Minkowski formulation. A paper by Gordon [19] argues that their results are dominantly affected by the force density gradient caused by the gaussian beam. A very similar experiment that was done recently is by Cui [20] with the addition of another layer of dielectric in-between the liquid-air interface. The experimental setup can be seen in Figure 5. The IR laser source used for the experiment is $3\,mW, 1{,}552.1\,nm$ laser connected to an erbium-doped attenuated optical fiber laser amplifier with the final radiation power adjustable between $0-300\,mW$, however as they noted most of the experiments were carried in the range of $0-200\,mW$.
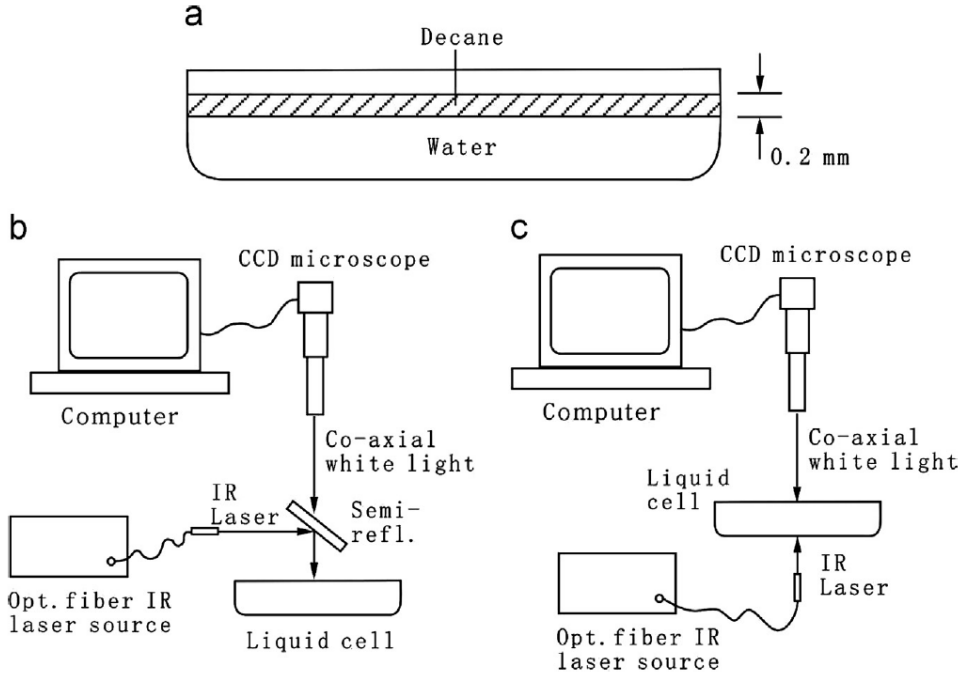
Figure 5: Experimental setup. (a) Two-layer liquid contained in the liquid cell; (b) top-incident configuration; and (c) bottom-incident configuration [20].

Depending on the momentum transfer at the media boundaries, either the decane layer will squeeze, in line with the Minkowski form prediction, or it will bulge outwards, which would be the predicted case for the Abraham form. Surprisingly their results are contrary to the Ashkin's, they observed a reduction in the thickness of the intermediate decane layer.

Gibson et al.'s paper, published in 1980 [21] measures the photon drag coefficients in both n- and p- type germanium and silicon in the far-infrared spectrum. In the long wavelength limit, predictions of the Minkowski form fit the experimental data observed.

One of the more recent and a bit controversial papers was published by She et al. in 2008 [3]. In the paper, they hung a nanometer silica fiber filament from top and measured the deflection optically using a camera when a light pulse is propagated through the fiber. Depending on the Abraham or Minkowski formulation, the theories predict that there will be a push or a pull force at the end of the fiber respectively.

The fiber in use is fabricated from a commercial single-mode SMF-28 fiber (Corning Company) using a method described in Tong's paper [31]. The fabricated fiber can be seen in Figure 6.
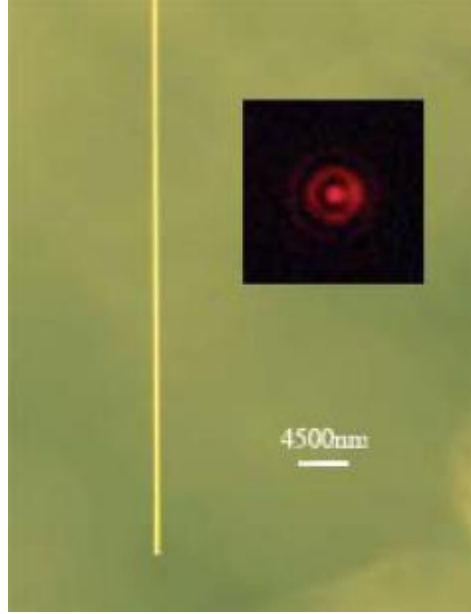

Figure 6: The stationary micrograph of the tip of the SF, showing that the diameter of the SF tip is about $450\ nm$. The inset is the enlarged profile of a weak red light beam outgoing from the SF end face [3].

As seen from Figure 6; the diameter of the filament used is $\sim450\ nm$. The light source used is an unpolarized $650\ nm$ semiconductor laser with a fiber connector with the option of supplying $10\ mW$ peak power in pulsed or continuous operation. In the pulse mode, the full duration of the pulse is reported as $4/15$ s followed by a dark interval of $1/5$ s. This laser is coupled to the fiber, which is $2\ m$ long in its entirety. The fiber assembly is mounted on a hermatic flat-circunal-shape glass container in order to minimize fluctuations from the air. The length of the fiber that is inside the container, which is the part free to move is $1\ cm$. The digital camera used to obtain the images (Canon G5) is shooting in the movie mode at 15 FPS. They measured the coupled power to the fiber after the experiments by cutting the fiber and taking off the coating. Figure 7 shows camera images obtained from the experiment. The coupled in peak power was measured to be 6.4 mW, with the deflection of the fiber $\Delta x \approx 9\ \mu m$.

13

The asymmetric bending apparently seen on the body of the filament indicates that a net push force acting on the end face since for a pull force, the predicted behavior is a simple deflection much like a small swing of a pendulum.

In order to minimize the effects of unwanted scattering, the transmission P_T, transmission plus scattering P_{T+S} and the transmission of the cut bare single-mode fiber P_{Fib} are measured using a universal optical meter (13 PDC 001, from MELLES GRIOT) with a 5 MM integrating sphere. The calculated results for these are $6.1547 \pm 0.0007, 6.1981 \pm 0.0003$ and 6.1973 ± 0.0001 mW respectively. To rule out any possible thermal effects, they attached a 3 μm colophony filament to the tip of the fiber and using the same laser in continous mode, waited for 60 minutes to observe whether the attached filament would heat up to the decomposition temperature of the colophony filamanet, which is near $300\,°C$. Since the thermal expansion coefficient for the silica fiber is very low ($\sim 5 \times 10^{-7}/°C$), they deem the thermal expansion to be insufficient to cause any observable movement of similar magnitude on the fiber. They also repeated the experiment in a vacuum of 2×10^{-5} Torr at $20\,°C$ with a 980 nm power-tunable, unpolarized semiconductor laser in continous mode. The results in vacuum can be seen in Figure 8. The numerical simulations in Figure 8 (A) & (B) parts are calculated using ANSYS 6.0 and the parameters used are given in the paper as; length $L = 5\,mm$, diameter $d = 520\,nm$, mass density $\rho = 2.2\ g/cm^3$, Young's elastic modulus $Y = 70\,GPa$ and refractive index $n = 1.451$. The optical push force is calculated via Eq.7a. [3]

$$f_A = \frac{2P}{nc}\frac{(n-1)}{(n+1)}$$ (Eq.7a)

In contrast, the predicted optical pull force by the Minkowski form is given in Eq.7b. [3]

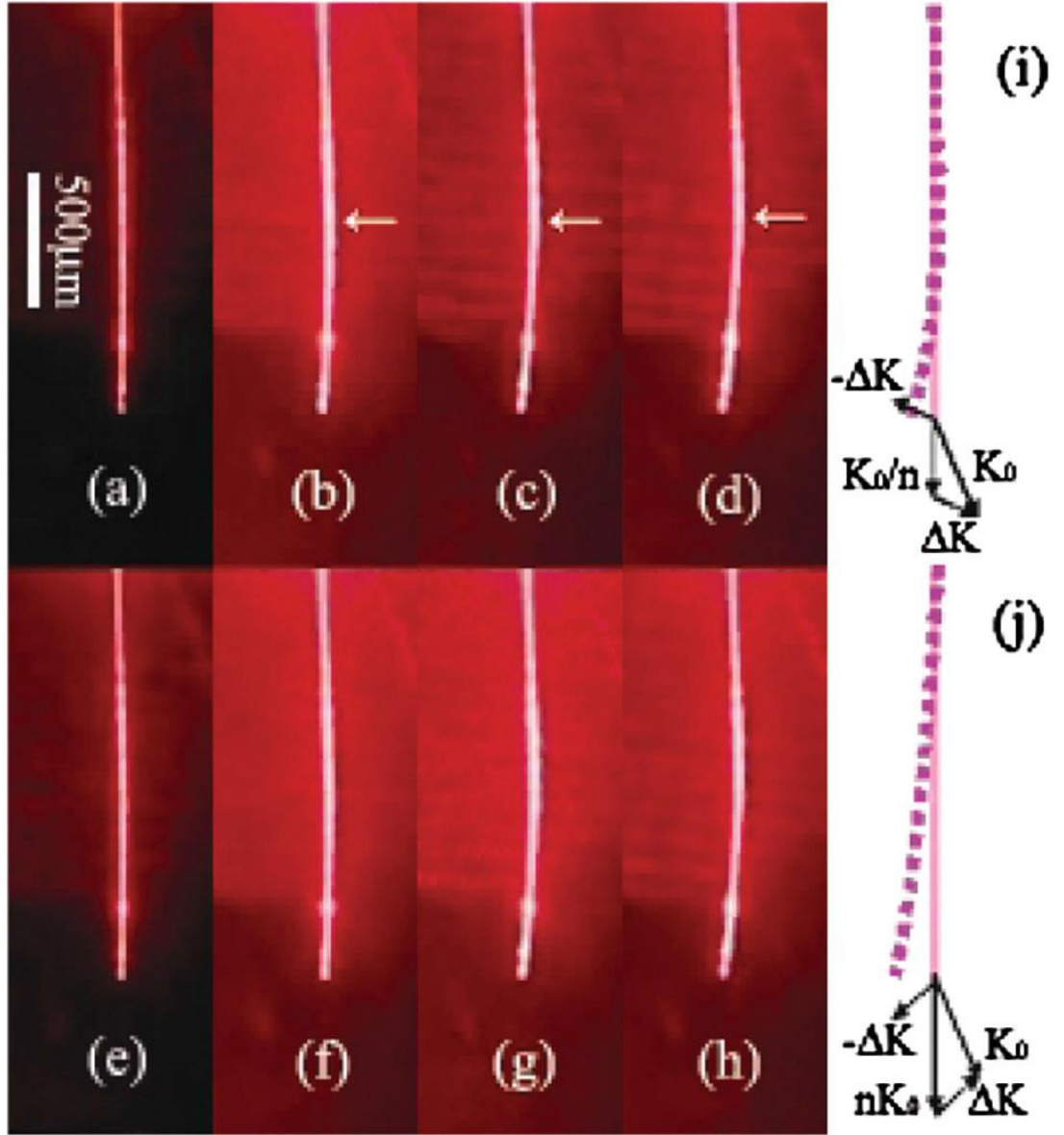$$f_M = \frac{2nP}{c}\frac{(n-1)}{(n+1)}$$ (Eq.7b)

14

Figure 7: The video frames of the moving SF as the result of the optical force for the SF in air, where (a), (b), (c) and (d) are the images of SF at 0, 1/15, 2/15 and 3/15 s, respectively, after a laser pulse arrives, and (e), (f), (g) and (h) correspond to the next laser pulse. Figures (i) and (j) show the effect of asymmetric refraction related, respectively, to Abraham momentum $\mathbf{K_0}/n$ and Minkowski momentum $n\mathbf{K_0}$, where $\mathbf{K_0}$ is the vacuum momentum of light and $\Delta\mathbf{K}$ ($-\Delta\mathbf{K}$) is the momentum change of light (SF end). Pink solid and dashed lines in (i) and (j) indicate two different states of the SF [3].
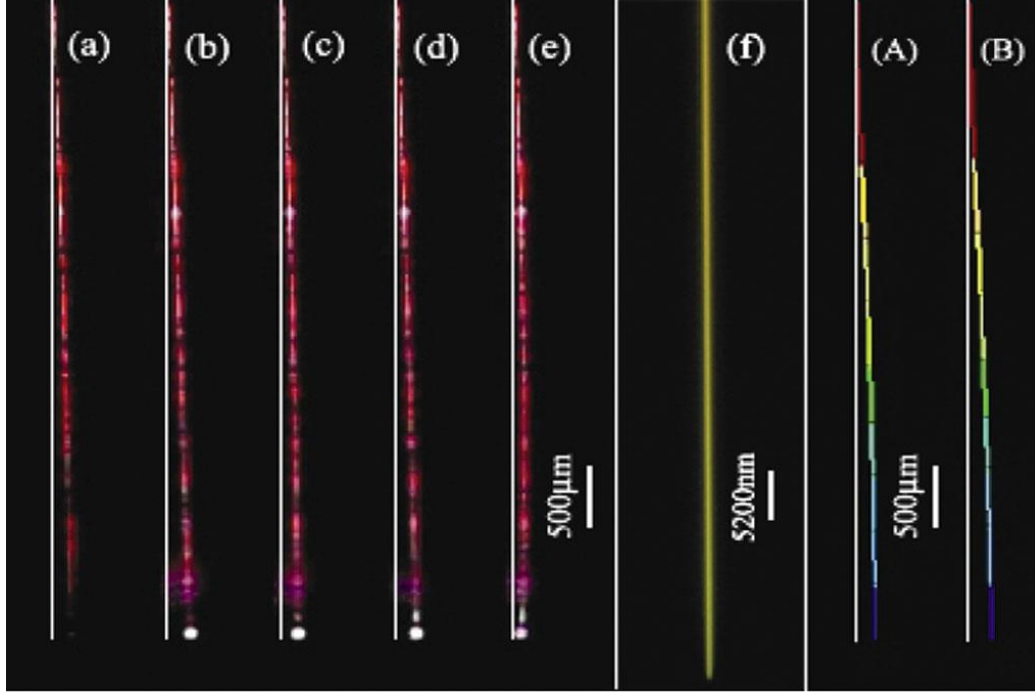
Figure 8: The video frames of the moving SF as the result of the optical force for the SF in a vacuum of 2×10^{-5} Torr at $20\,°C$ with an electrostatic shield. The SF is driven by a power-tunable, unpolarized cw $980\,nm$ light and higlighted by a $0.1\,mW$ cw $650\,nm$ light. (a) No $980\,nm$ light is coupled in; (b) the coupled-in power of $980\,nm$ is $17.8\,mW$; (c)-(e) the power is increased further to $19.5\,mW$ in a time of $1.9\,s$; (f) the micrograph of the SF tip. Figures (A) and (B) are the results of the numerical simulations, with (A) corresponding to the inital state (a) and (B) corresponding to (b). The white vertical lines are for displacement reference [3].

CHAPTER II

EXPERIMENTAL DESIGN

The experimental setup used in this thesis is similar in idea to the setup used by She et al. [3], albeit different in techniques of measurement and the method used for displacing the fiber. Instead of sending pulses to a comparably long and thin fiber filament, a thicker and shorter fiber is manufactured with an angle on the exiting end and a constantly modulated laser is used for displacing the fiber. The excited fiber will behave as a driven harmonic oscillator and can be modelled as a cantilever supported at one end using Euler-Bernoulli beam theory. For resonances with a high quality factor Q, the displacement caused by the modulation will be Q times higher, increasing the expected displacement in to a range suitably measureable by an interferometer. A fiber interferometer can be used to measure the total displacement of the excited fiber, while the laser of another fiber interferometer, modified to accept modulation from a signal source can be used for excitation.

II.1 Classical Model

The fiber used for the deflection measurement is modeled as a cylindrical cantilever with a spring constant k, and a fundamental frequency f_0. The fiber used for the experiment is SMF-28, manufactured by Corning with $d = 125 \pm 0.7 \, \mu m$ as the cladding diameter [32], with the Young's modulus $Y = 73.1 \, GPa$ and mass density $\rho = 2.203 \, g/cm^3$. The relevant equations for k & f_0 are given in Eq.8a & 8b.

$$k = \frac{3YI}{l^3} \qquad\qquad \text{(Eq.8a)}$$

$$f_i = \frac{C_i}{2\pi}\sqrt{\frac{k}{0.24m_c}} \qquad\qquad \text{(Eq.8b)}$$

Where $I = \pi d^4/64$ in Eq.8a denotes the moment of inertia and m_c denotes the total mass of the cantilever which can be calculated easily for any given values of length l. For the fundamental frequency f_0, C_0 is simply equal to 1. Note that the spring constant calculated here is for the lateral movement of the fiber; that is, for displacements perpendicular to the symmetry axis defining the cylinder. Simply using the Hooke's law $F = -kx$ we can estimate the total amount of force subjected on the fiber by the outgoing light by measuring the deflection if we know k. Since the end face of the fiber that is used in this thesis is angled at a certain degree by hand (method of achieving this is discussed in Chapter III), the net lateral force will depend on this angle. The momentum components at the end face are illustrated in Figure 9:
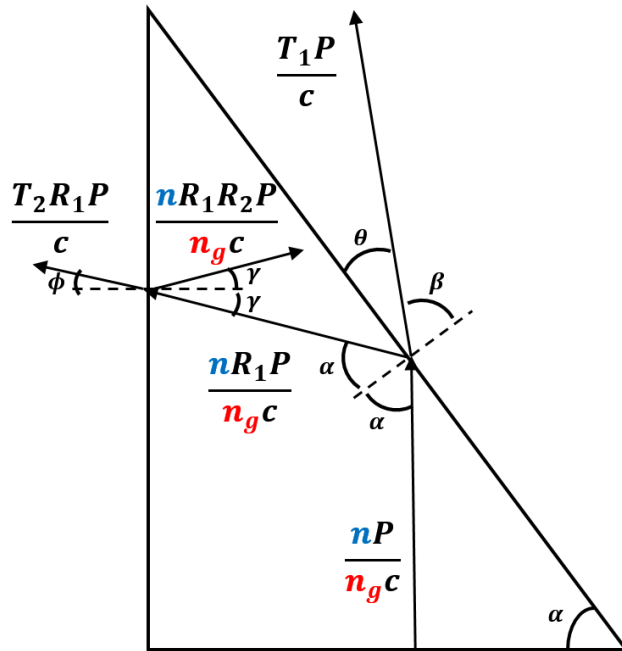

Figure 9: Momentum components at the end face of the angled fiber, blue (n) parts depict the Minkowski case and the red (n_g) parts depict the Abraham case values.

If the displacement of the fiber can be measured when a light pulse is exiting, the affecting force can be calculated for both the Abraham and Minkowski forms of the momentum and be compared with the measured values.

II.2 Calculations

The calculated f_0 and k values for a given length of fiber l is plotted in Figures 10 & 11 respectively using Eq's 8a and 8b.
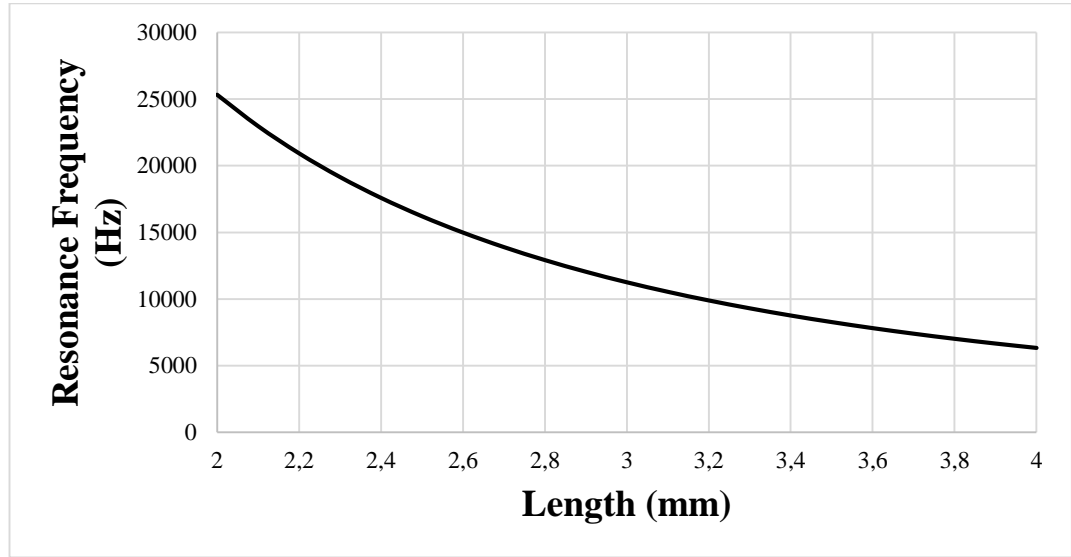

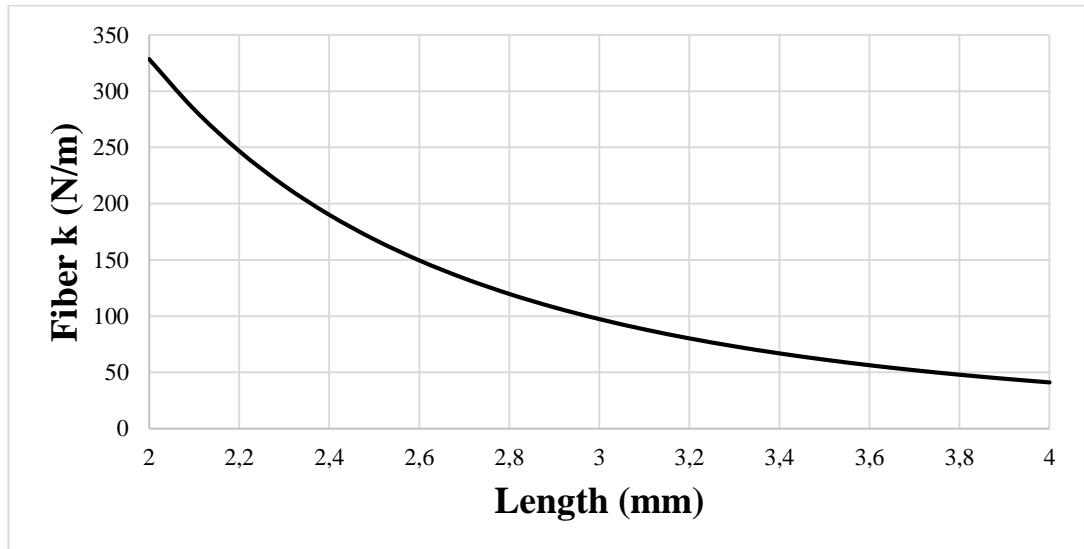Figure 10: f_0 values calculated using Eq.8b with respect to the fiber length l.

Figure 11: k values calculated using Eq.8a with respect to the fiber length l.

19

The reflection and transmission coefficients R and T shown in Figure 9 can be calculated using the Fresnel Equations for s and p polarizations. Since the polarization is not maintained inside the excited fiber, we have assumed that the excitation beam consists of equal parts of s and p polarizations and use the average in calculating the coefficients R and T. Total angle of the transmitted signal with respect to the horizontal axis is simply given by $\theta = \alpha + (90 - \beta)$. Eq. 9a and Eq. 9b show the predicted lateral force at the fiber end face for the Abraham and the Minkowski case respectively, where we utilized the conservation of momentum to calculate the transfer assuming that the light reflected from the angled end face of the fiber reflects once more inside the fiber.

$$F_A = T_1 \frac{P\cos\theta}{c} + R_1 \frac{P\cos\gamma}{n_g c} + T_2 R_1 \frac{P\cos\phi}{c} - R_2 R_1 \frac{P\cos\gamma}{n_g c} \qquad \text{(Eq.9a)}$$

$$F_M = T_1 \frac{P\cos\theta}{c} + R_1 n \frac{P\cos\gamma}{c} + T_2 R_1 \frac{P\cos\phi}{c} - R_2 R_1 n \frac{P\cos\gamma}{c} \qquad \text{(Eq.9b)}$$

Since the momentum attributed to the light inside the fiber is larger than that in the outside medium for the Minkowski case, there is pull-force going from a higher index medium to a lower index medium, whereas the Abraham case predicts a push force. However, for our experimental setup, the dominant force is the reaction of the fiber to the radiation pressure force of the first reflected beam so no change of direction between two theories is expected.

The displacements calculated for the Minkowski and Abraham cases, for the fibers cleaved at an angle of 43° are plotted against various l values in Figure 12 as displacement per mW of laser power. The first Fresnel coefficients are $T_s = 0.293, R_s = 0.707, T_p = 0.526, R_p = 0.474$. The angle of the transmitted signal with respect to the surface normal is $\approx 84.7°$ thus the total lateral angle of the transmitted signal $\theta \cong 48°$ The average $T = 0.41$ and $R = 0.59$.
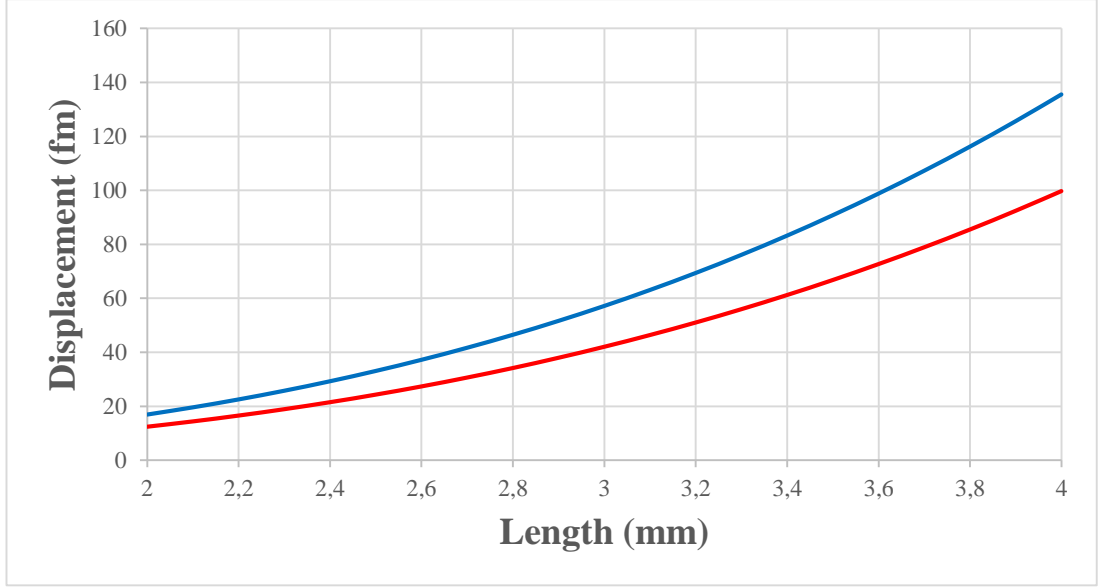
Figure 12: Displacement calculated for a fiber angled at $43°$ and with length varying between $2 - 4\,mm$ for $1\,mW$ laser power. Predicted values for the Minkowski case is shown in blue whereas the Abraham case is shown in red.

The same calculations for the Minkowski and Abraham cases, for a fiber cleaved at an angle of $35°$ are plotted against various l values for per mW laser power can be seen in Figure 13. The first Fresnel coefficients are $T_s = 0.861, R_s = 0.139, T_p = 0.999, R_p = 0.001$. The angle of the transmitted signal with respect to the surface normal is $\approx 56.9°$ thus the total lateral angle of the transmitted signal $\theta \cong 91.9°$. The average $T = 0.930$ and $R = 0.07$.

As seen from the Figures 12 and 13, the expected displacement due to either of the forces are in the $10^{1-2}\,fm$ range. Using an all fiber interferometer manufactured by Nanomagnetics Instruments which has a noise floor of $20\,fm/\sqrt{Hz}$, measuring these displacement values near a resonance with high quality factor does not seem far-fetched. The measurement fiber might be aligned to the excited fiber to detect the displacement.
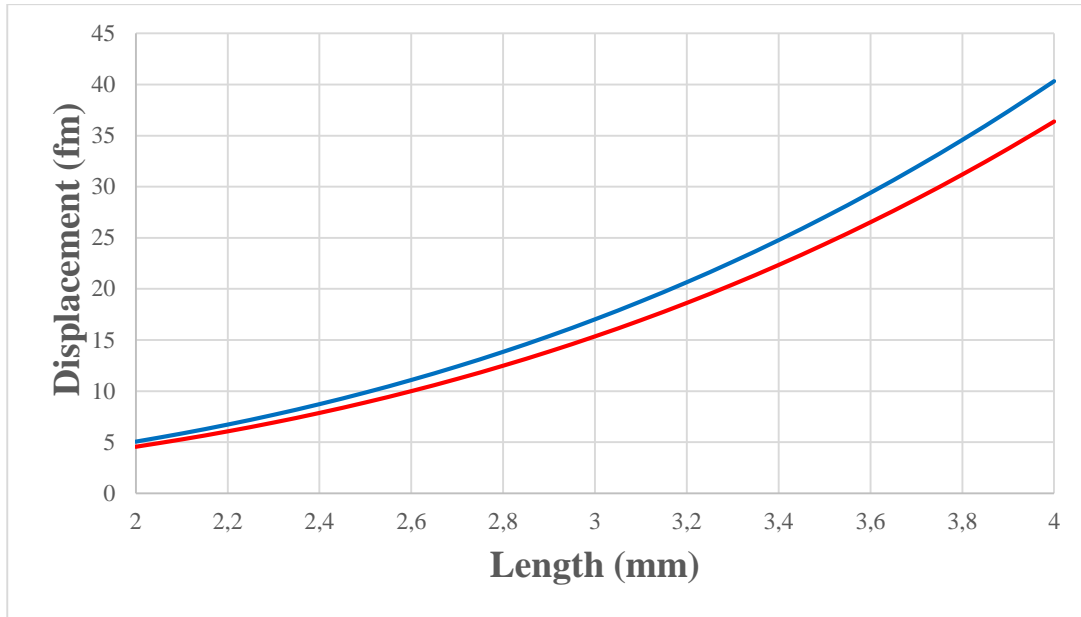
Figure 13: Displacement calculated for a fiber angled at 35° and with length varying between $2 - 4\,mm$ for $1\,mW$ laser power. Predicted values for the Minkowski case is shown in blue whereas the Abraham case is shown in red.

CHAPTER III

EXPERIMENTAL SETUP

There are two fibers used utilized in the experimental setup, one of them is the fiber coming from the measurement interferometer which has its output connected to a SR830 Lock-In Amplifier (Stanford Research Systems) and a FSV Signal Analyzer (Rohde & Schwarz) for taking measurements. The other fiber is the excited fiber which is aligned perpendicularly to the measurement fiber and the laser excitation is accomplished by using an USB interferometer modified to accept an on-off TTL signal from the SR830 Lock-In Amplifier. The measurement and excitation interferometer is controlled using their respective software and the measurements are taken using MATLAB via RS232 from the Lock-In and the ASCII export function of the Signal Analyzer. The mechanical assembly sits on top of a vibration isolation table attached to an optical breadboard with 3 micrometer stages for spatial alignment. The fibers are first fed through modified syringe needles and firmly held in place by a liquid adhesive that is applied carefully as not to coat the fiber filaments. The angle polish of the excited fibers is done after the fiber is mounted on the needles to ensure no chipping or breaking occurs during the feed through.

III.1 Schematic

An overview of the experimental setup is given as a block diagram in Figure 14. The angled fiber and the interferometer fiber that is used to measure the displacement sits on top of a vibration isolation table manufactured by Minus-K Technology. The alignment is controlled by X, Y and Z stages with 3 degrees of freedom.
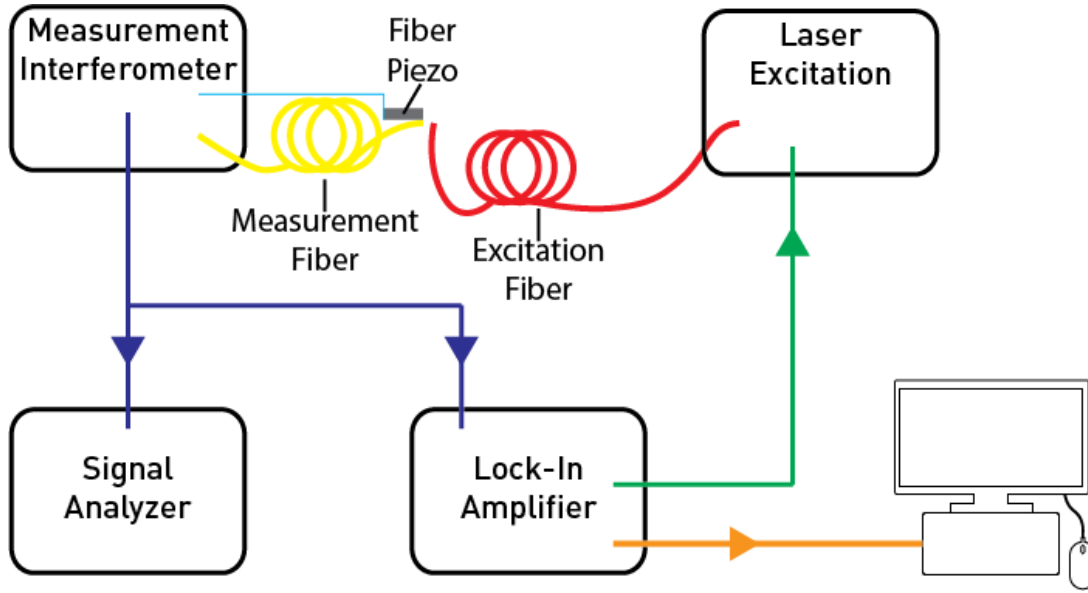
Figure 14: Overview of the experimental setup. The measurement interferometer output can be measured either by the A input of the Lock-In, or by the Signal Analyzer with a DC blocker in front of the input. The signal for excitation amplitude is controlled via the TTL-Out port on the back of the Lock-In. The Lock-In Amplifier is controlled using MATLAB via the RS232 interface.

The fiber used for the measurement is mounted on the X-Y stages whereas the fiber that is being measured is mounted on the Z stage since vertical adjustments are needed less frequently for maintaining proper alignment. General view of the aligned fibers can be seen in Figure 15. The measurement fiber is connected to an interferometer manufactured by Nanomagnetics Instruments with a noise floor of $20\ fm/\sqrt{Hz}$, which can be seen mounted in a rack system in Figure 16.

Output of the measurement interferometer is sent to the A input of a SR830 Lock-In Amplifier. A BNC T-connector is used to send the same signal to the input of a FSV Signal Analyzer with a DC blocker attached before the input. The interferometer used to excite the angled fiber is a USB-connected all fiber interferometer manufactured by Nanomagnetics Instruments which is modified so that the TTL-Out signal from the back of the SR830 will modulate the power of the laser and can be seen in Figure 17.
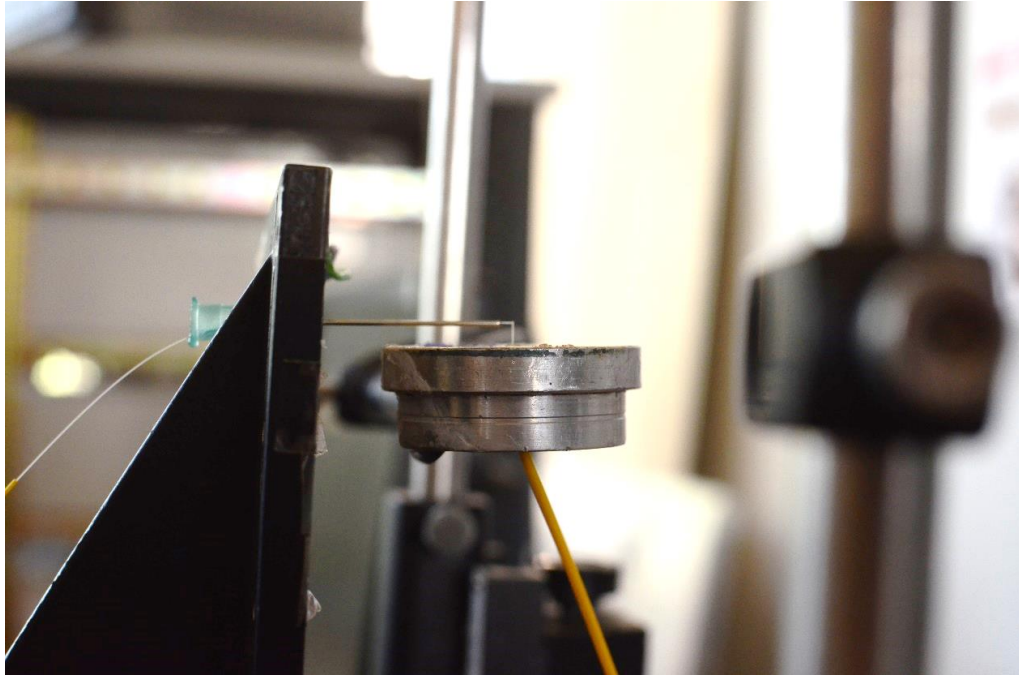
Figure 15: Measurement interferometer fiber (left) is in alignment with the excited fiber (center)
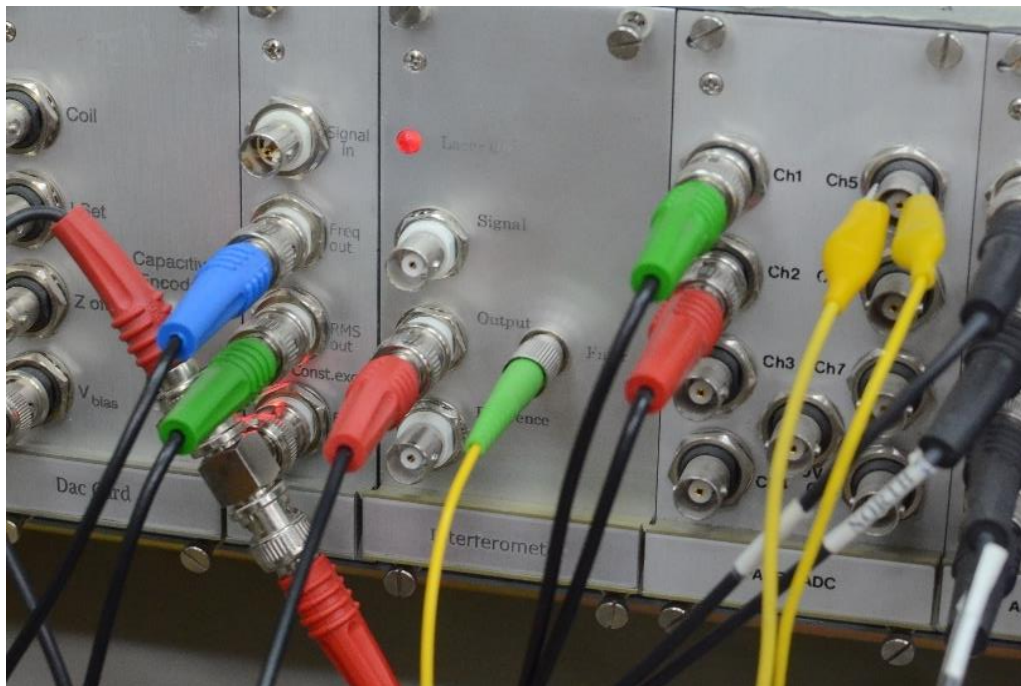

Figure 16: Nanomagnetics Instruments Fiber Interferometer

Reference output of the excitation output is monitored using an oscilloscope to measure the power delivered to the photodiode.

The SR830 Lock-In amplifier is controlled through a PC via RS-232, the MATLAB code used for controlling the Lock-In is given in Appendix A. Total amplitude R and the phase θ are captured using the SNAP command rather than OUTP command to make sure that the data is read at the same time rather than successively. The details describing the behavior of commands can be found in the SR830 Reference Manual [33].
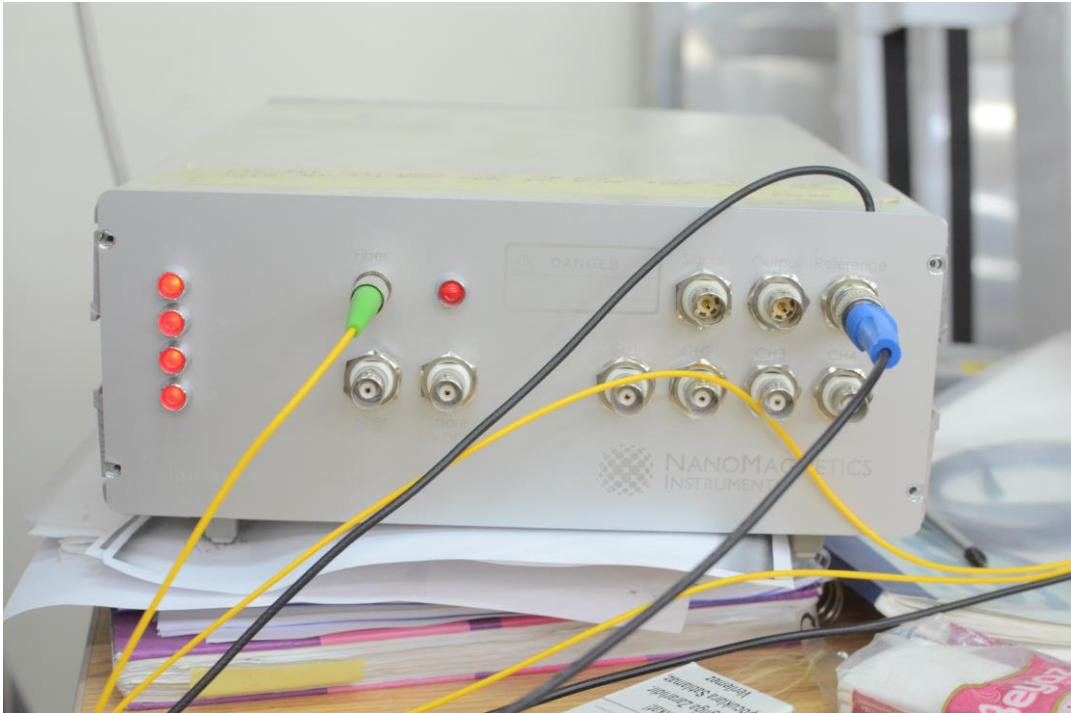

Figure 17: Nanomagnetics Instruments USB Fiber Interferometer, modified for modulation using a TTL signal. The TTL-Out connection coming from the Lock-In can be seen going inside the chassis.

III.2 Manufacturing the Angled Fiber

The angle of the fiber end face is carefully manufactured under a stereoscopic microscope with the base fiber being a single-mode SMF-28 fiber manufactured by Corning. After stripping to the desired length, the end of the fiber is slowly subjected to three successive grades of polishing. An Aluminum Oxide Latex paper of ISO grit size P800 and Silicon Carbide Electro Coated abrasive paper with ISO grit size P1500 is used for determining the rough angle and eliminate possible chirp and cracks on the end from stripping. The grit sizes correspond roughly to an average particle diameter of $21.8 \, \mu m$ and $12.6 \, \mu m$ respectively. The final polishing is done using a Fiber Polishing Paper from Thorlabs having the average particle diameter of $3 \, \mu m$. The process steps are pictured in Figure 18. For angles smaller than $40°$, the flexing of the fiber does not allow sufficient friction for the final polishing to be even. In order to achieve a smooth end face for lower angles, the fiber is mounted on a drill bit and held securely by the cladding while the polishing paper is carefully scraped upon the end face. End result of the polishing process can be seen in Figure 19.
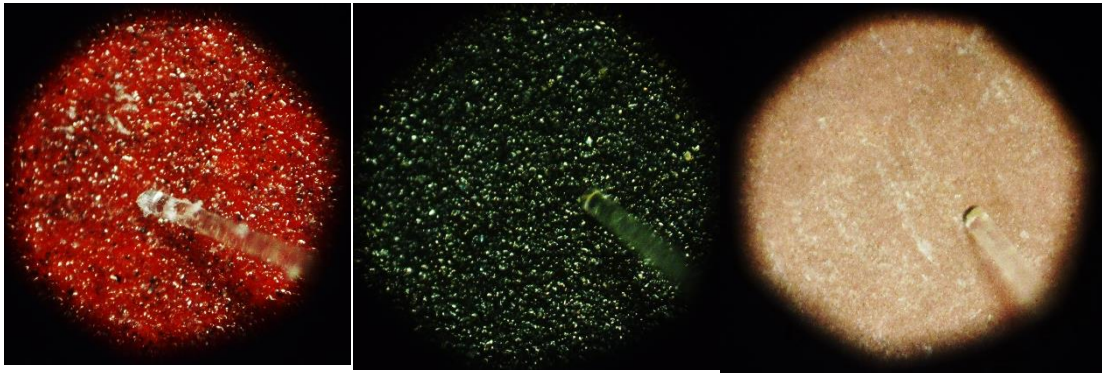

Figure 18: Forming and polishing the angled end of the fiber. The fiber is rubbed against successive abrasive surfaces to form and maintain a smooth angled end
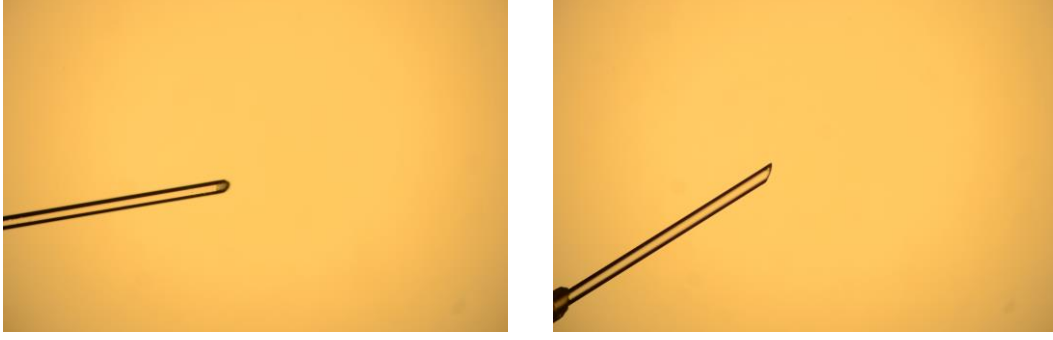
Figure 19: Final polished end of the fiber filament

The corresponding angle calculated from the taken pictures for this particular fiber is $\approx 45.6°$. The specifications given for the fiber from the manufacturer are cladding diameter $d = 125 \pm 0.7\ \mu m$ with the Young's modulus $Y = 73.1\ GPa$, index of refraction $n_g \cong n = 1.4682$ at $1{,}310\ nm$ since the zero dispersion wavelength of the fiber is $\lambda = 1{,}304\ nm$, and mass density $\rho = 2.203\ g/cm^3$.

III.3 Measurements

The fabricated fibers are fixed on a custom mechanical holder using an adhesive to affix the fibers. The liquid adhesive is deposited carefully and the process is monitored through a stereoscopic microscope in order to make sure no adhesive coats the fiber. One of the fibers used for the measurement can be seen in Figure 20, with a ruler for reference. The fibers are first measured using a piezo speaker divided in half between the $0 - 20\ kHz$ range with $10\ Hz$ resolution for mechanical resonances. The attached piezo can be seen in Figure 21. The driving signal is supplied from the Sine Out of the Lock-In, which is at the same frequency as the internal clock of the Lock-In and with a set amplitude between $4 - 100\ mV$ connected to two halves of the speaker while the ground connection is left floating. The Lock-In settings used for taking the piezo actuated data are as follows for the $0 - 20\ kHz$ range: Signal Input: A with AC coupling and Floating ground, Time Constant $\tau = 10\ ms$, Sensitivity: $1\ V$, Reserve: *Low Noise*, RC Filter: $-24\ dB$. Both the Line and the Line x 2 filters are on throughout the measurements. During this time the TTL-Out going into the excitation interferometer is disconnected, which turns the excitation laser off.
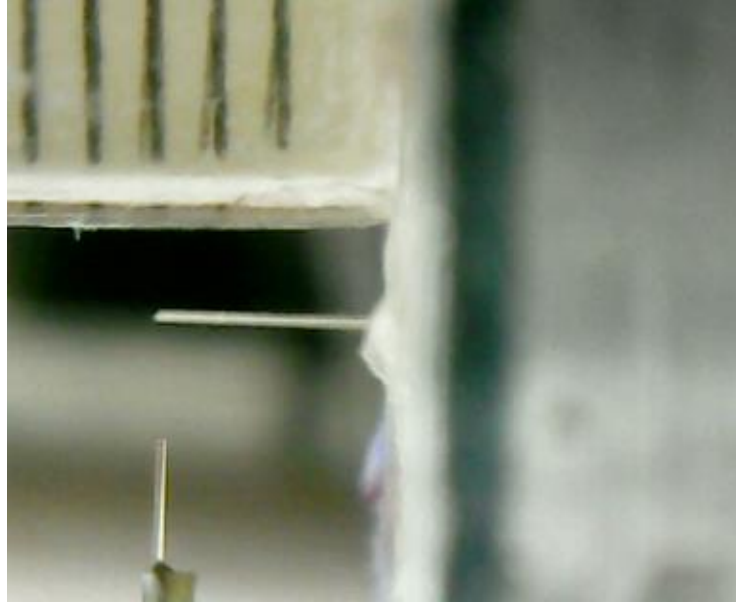
Figure 20: Method of measuring the length of the affixed fibers

After the piezo actuation, the piezo speaker is disconnected and the TTL-Out is connected back again to the excitation interferometer to scan the $0-20\ kHz$ range with $10\ Hz$ resolution, then possible peaks are scanned later with a $1\ Hz$ resolution using the appropriate sensitivity $(100\ \mu V - 1\ V)$ with and without the fiber near the measurement interferometer to eliminate the peaks caused by possible electrical noise and other mechanical vibrations. In order to Lock-In to settle to a correct value, the software waits for at least $10\ \tau$ before taking any measurements at a given frequency. Remaining resonance peaks and their vicinities are scanned by hand to find the most responsive frequency. At the found frequency, the Lock-In reserve is set to $High\ Reserve$, the sensitivity is set to $10\ mV$ and the Time Constant is set to $30\ s$ to measure the output of the measurement interferometer while the excitation laser power is controlled through the software as a percentage. The reference voltage of the excitation interferometer is also monitored and stored during the measurements using an oscilloscope. During the Lock-In measurements, the BNC T-connector on the input, which also carries the signal to the Signal Analyzer is removed from its place. After the measurements are done, the Signal Analyzer is connected and both values are measured again between $0-100\%$ laser power with 10% increments. The Signal Analyzer has a bandwith resolution of $1\ Hz$, the center frequency is the same as the

29

excitation frequency with a span of $1\ kHz$ around the center frequency. The sweep points are set to 1,000 points and the sweep count is 100. The measured voltage values are then divided by the respective slopes of the measurement interferometer to deduce the total displacement of the excited fiber.
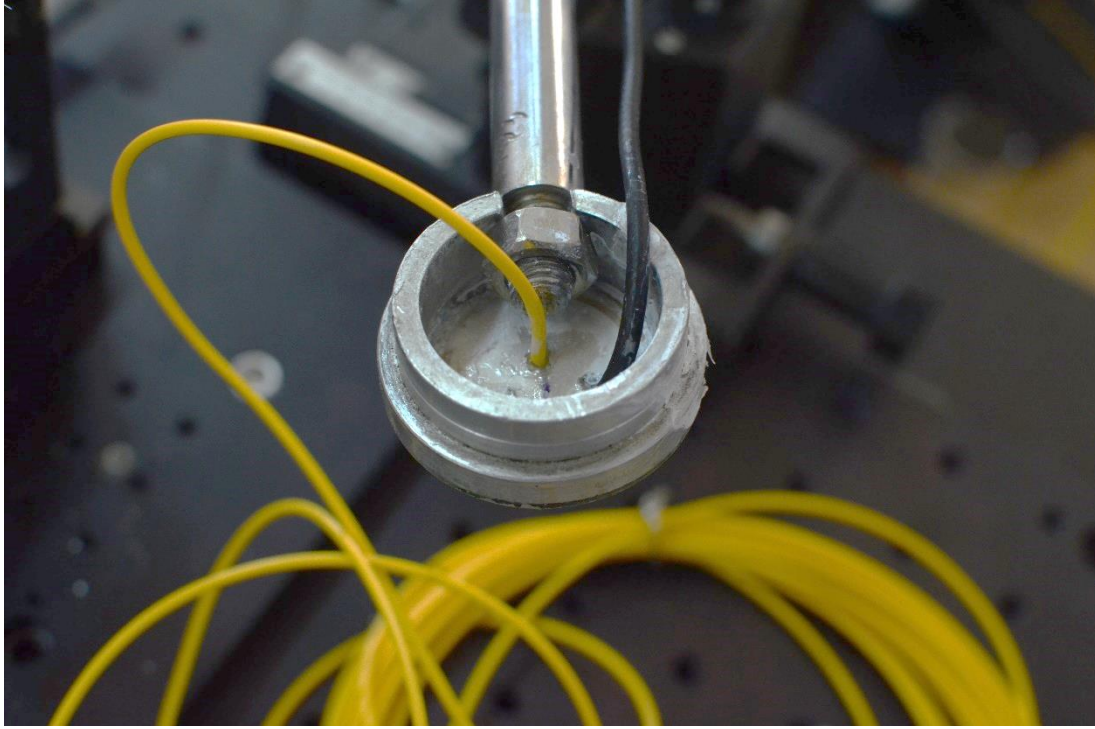

Figure 21: The measured fiber goes through a hole in the center of a piezo speaker which is divided in half. The fiber end face orientation is normal to the line dividing the piezo speaker which is aligned in the same plane as the measurement interferometer.

CHAPTER IV

EXPERIMENTAL DATA

The experimental data for the first measured fiber is presented below. The piezo actuation data taken with the Lock-In can be seen in Figure 22. Lock-In is set to low noise reserve with $\tau = 10ms$ and the sensitivity is set to $1\,V$. Since the fiber is no longer cylindrically symmetric after the angling process, the movement along the direction of the angled face normal and the movement perpendicular to it will split into two slightly different modes of resonance. The distance between the cylindrical boundary of the fiber and the measurement interferometer varies as $\cos\varphi$ for movement along the perpendicular direction, which is negligible for small deflections expected for laser excitation but observable for larger deflections such as those caused by the piezo excitation. The fiber end face is angled approximately at $39.8 - 41.2°$ as calculated from the microscope images. Figure 23 shows the fiber extruding from the cut piezo speaker which is attached to the post holder. The length of the fiber, calculated from the microscope images is $3.8 \pm 0.05\,mm$. For this length, the fundamental resonance is calculated to be between $6,834 - 7,203\,Hz$ using Eq. 8a and Eq. 8b. Scanning around the peaks manually determined that the highest values recorded by both the Lock-In and the Signal Analyzer occurred at the excitation frequency of $6,877\,Hz$. The excitation laser power is modulated between $0 - 100\%$ settings using the interferometer software. The reference voltage output was also monitored using an oscilloscope, the waveforms are noticeably distorted from a square-wave for lower powers however for higher powers this difference is slight.
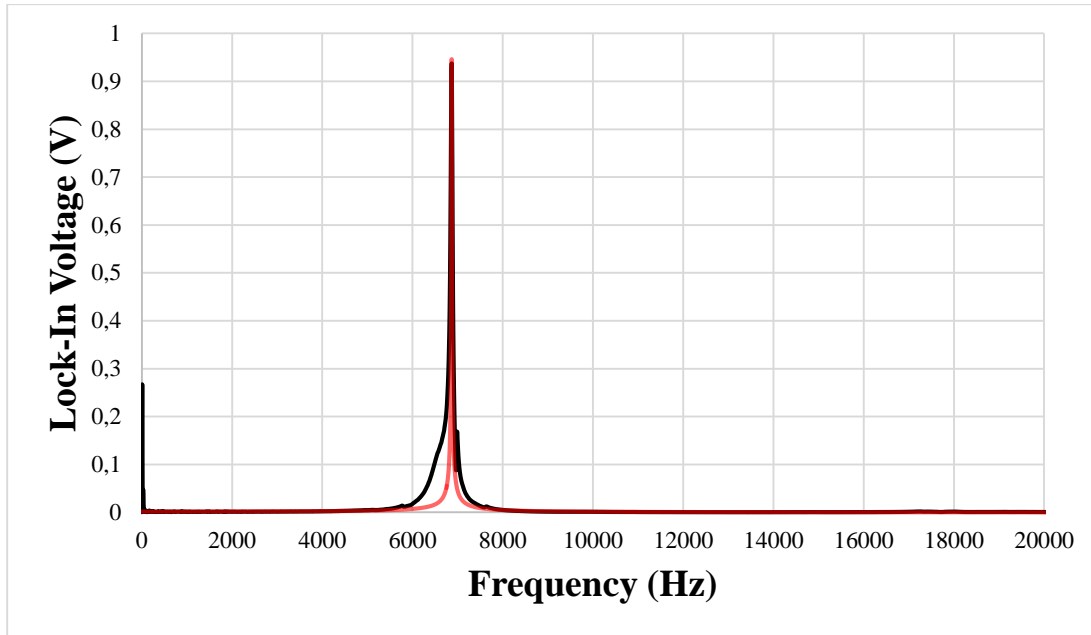
31

Figure 22: Amplitude data read from SR830 Lock-In Amplifier for piezo actuation of the first fiber with $40\ mV$ driving signal. Main peak is located near $6{,}877\ Hz$. There is a smaller peak near $7{,}000\ Hz$, which is possibly the fiber resonance perpendicular to the direction of measurement. The fit used for calculating the quality factor can be seen in red, $Q = 860$.
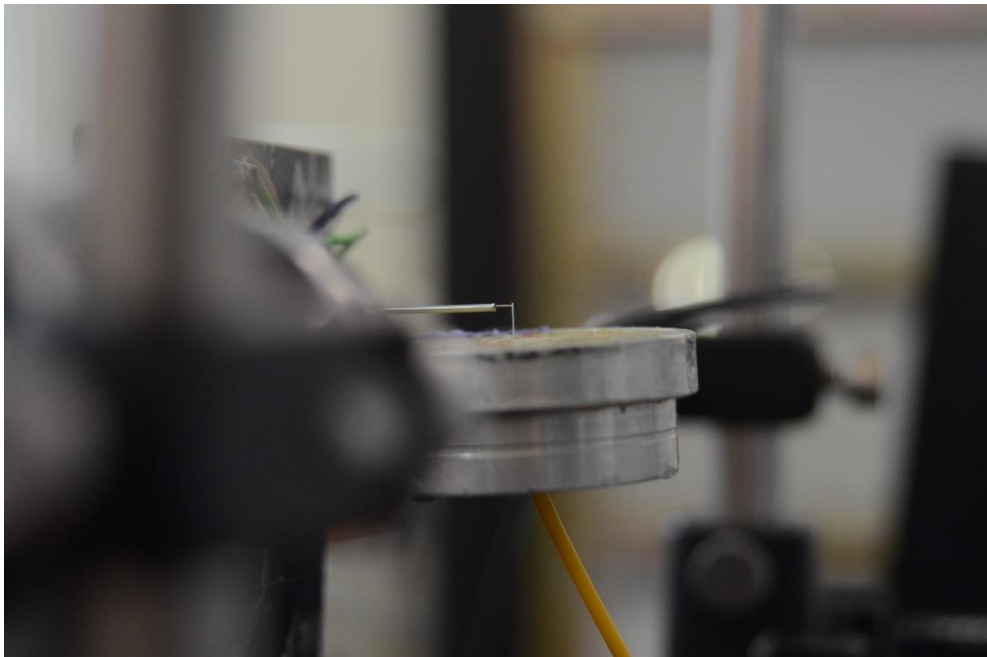

Figure 23: The mechanical assembly for the measurement of the first fiber. The piezo actuation is done by the piezo speaker divided in half through which the fiber feeds through.
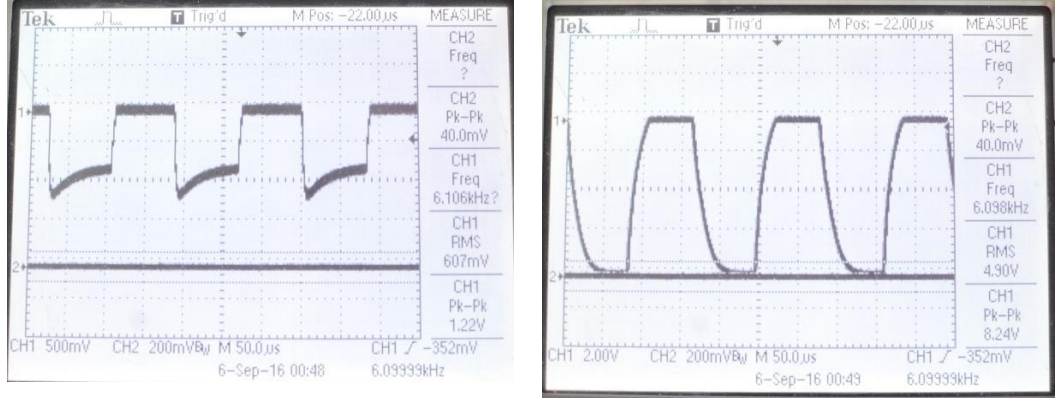
Figure 24: Shapes of the reference voltage of the interferometer used for excitation when driven by the TTL signal. Left image is for 10% power and the right image is for 100% power

Comparison of the waveforms at lower and higher powers can be seen in Figure 24. The data is first taken only using the SR830 Lock-In amplifier, and then using both the Lock-In, and the Signal Analyzer simultaneously. For laser excitation measurements, the Lock-In reserve is set to high reserve and the time constant τ of the Lock-In amplifier is set to $30 \, s$, which necessitates a waiting time of at least $300 \, s$ for each measurement in order to read accurate results. The sensitivity is set to $10 \, mV$ with the other settings as stated in section III.3. The Signal Analyzer is taking 1,000 sweep points with a 100 sweep count. Total power of the excitation is calculated using the reference voltage read from the photodiode, the responsivity is $1 \, A/V$ connected via a $3,000 \, \Omega$ resistor means that $P_{pd} = \frac{V_{ref}}{3000}$; however, there is also a 2x2 coupler inside the interferometer which will cut the delivered power to the half of the calculated value of P_{pd} which is included in the calculations. Measured RMS voltage values from the Lock-In amplifier are converted into displacement by dividing with the respective slope of the measurement interferometer at the time of the measurement. One of the slopes used in the measurement, namely the slope for the 100% excitation measurement, is shown in Figure 25. Displacement vs excitation laser power are given in Figure 26 with the Signal Analyzer unconnected to the Lock-In amplifier. The quality factors of the resonances are measured from the piezo actuation data by fitting a Lorentzian curve as seen in Figure 22. Figure 27 shows the Lock-In data taken during laser excitation of the fiber.
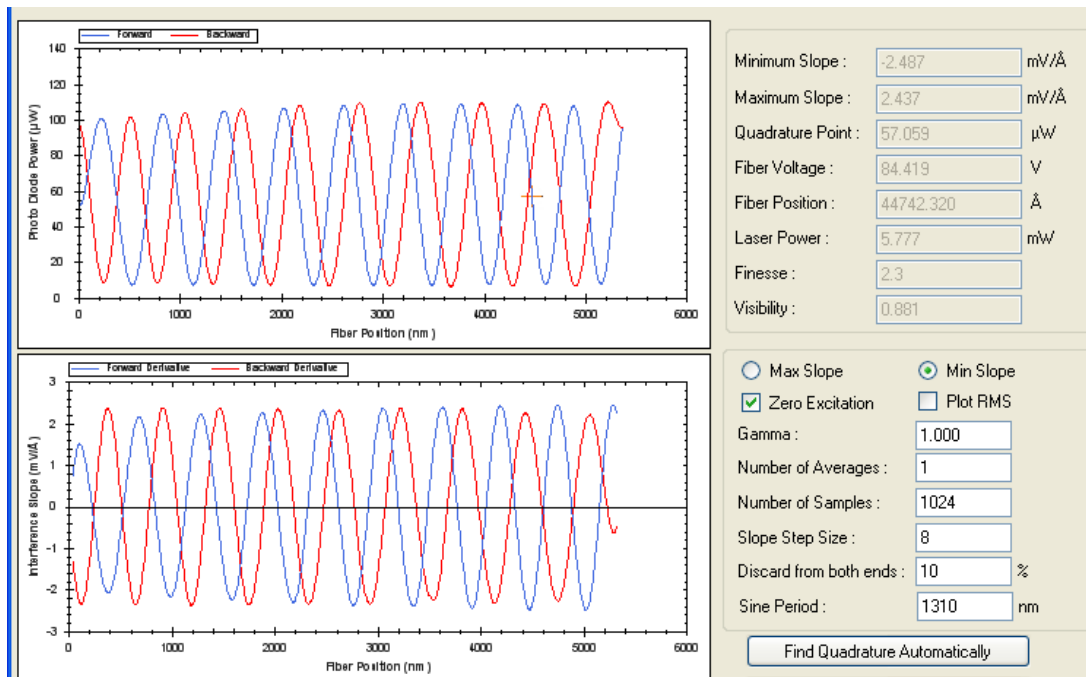
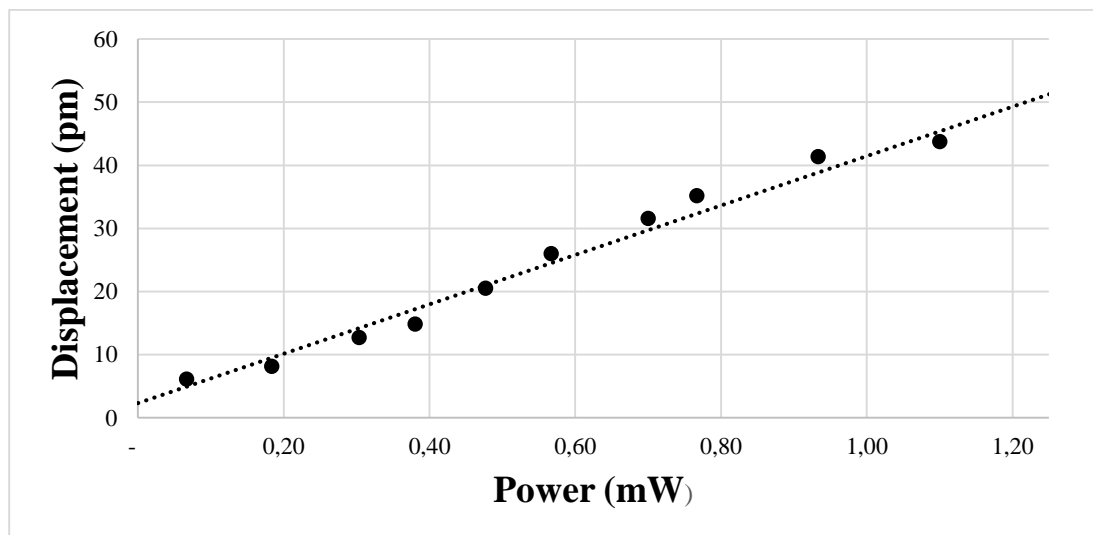Figure 25: Shape of an interference slope

Figure 26: Displacement in pm is plotted against the excitation laser power with a linear fit.
Output of the measurement interferometer is connected only to the Lock-In input.
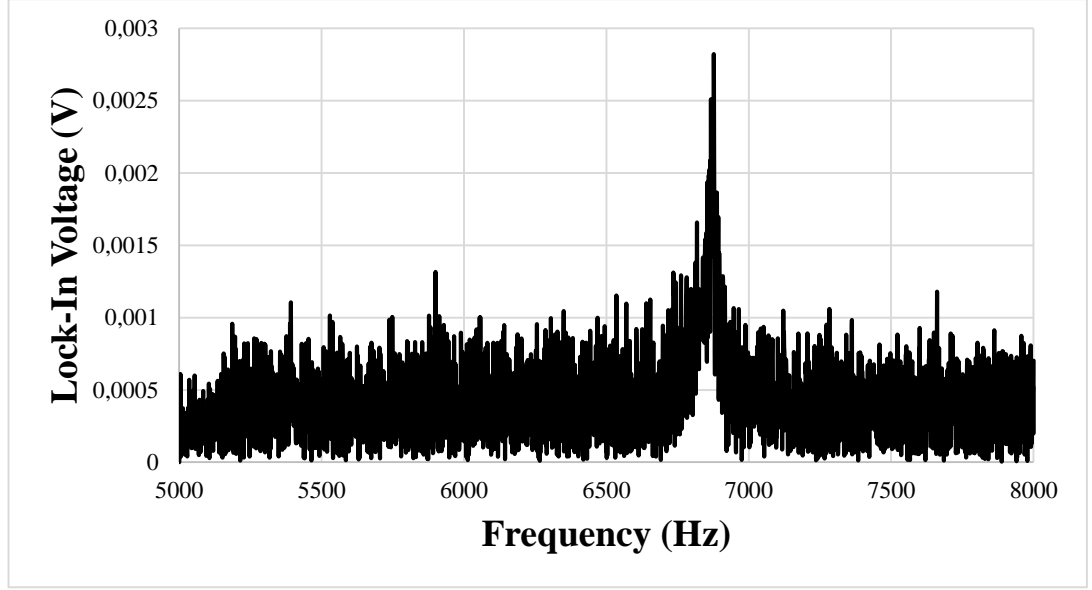
Figure 27: Lock-In data during laser excitation of the first fiber taken with $1\ Hz$ resolution, $\tau = 1\ s$ and sensitivity set to $10\ mV$.

For the second fiber, the piezo actuation data taken from the Lock-In with $\tau = 10\ ms$ and sensitivity set to $1\ V$ can be seen in Figure 28. The end face of the second fiber is angled between $28 - 32°$ as calculated from the microscope images. Figure 29 shows a close up of the fiber before smoothing the end face, the measured length corresponds to $3.85 \pm 0.5\ mm$ along with f_0 between $6{,}660 - 7{,}015\ Hz$. Scanning around the peaks manually determined that the highest values recorded by both the Lock-In and the Signal Analyzer occurred at the excitation frequency of $6{,}920\ Hz$. The excitation laser power is again modulated between the $0 - 100\%$ settings using the interferometer software. The slope of the measurement interferometer for the data at maximum power can be seen in Figure 30. Displacement versus excitation laser power is given in Figure 31 with the Signal Analyzer disconnected while the Lock-In amplifier is measuring with $\tau = 30\ s$ and sensitivity set to $10\ mV$. The fitting curve used for the quality factor calculation can be found in Figure 28. Laser excitation data from the Lock-In is shown in Figure 32.
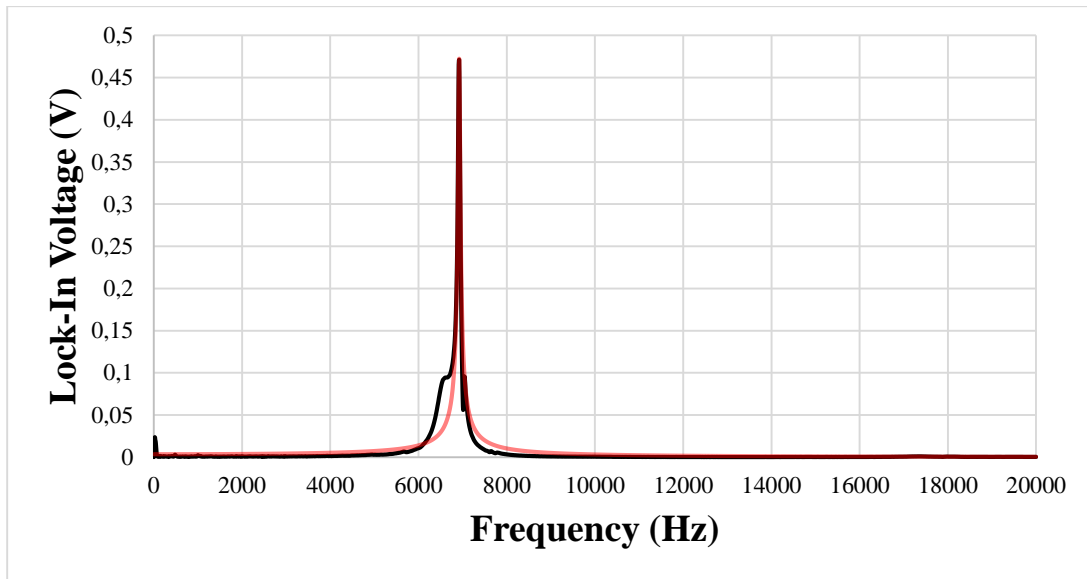
35

Figure 28: Amplitude data read from SR830 Lock-In Amplifier for piezo actuation of the second fiber with 100mV driving signal. The fit used for calculating the quality factor can be seen in red, $Q = 135$.

Figure 29: Close up of the second fiber used for taking measurements.
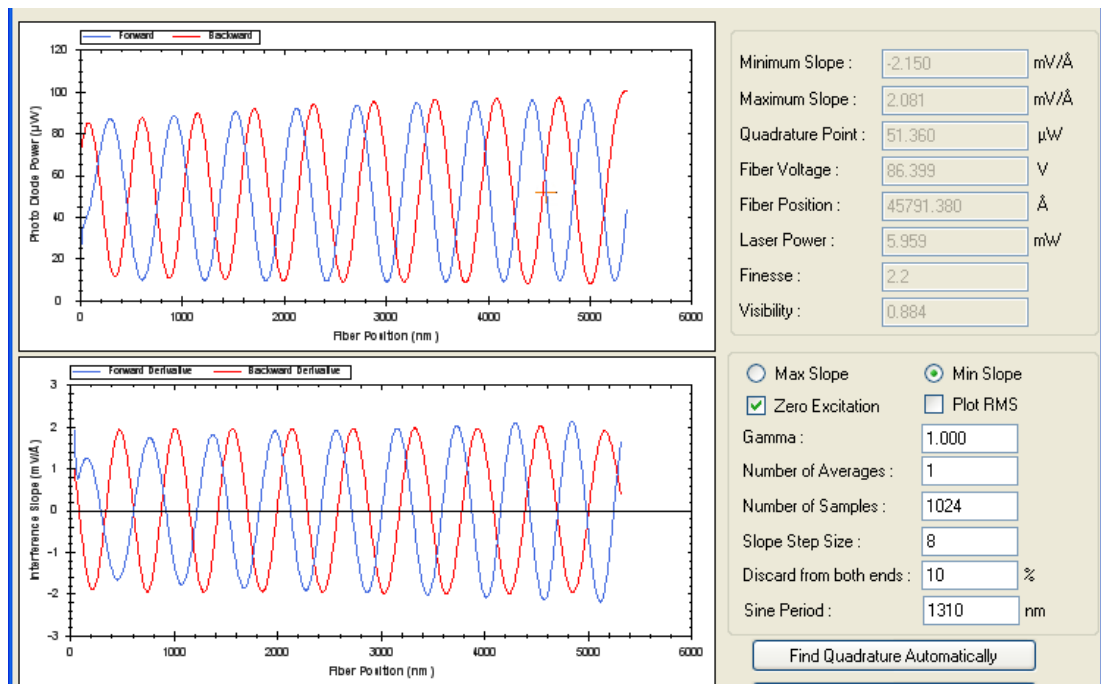
Figure 30: Measurement interferometer slope for the data taken at the 100% excitation of the laser.
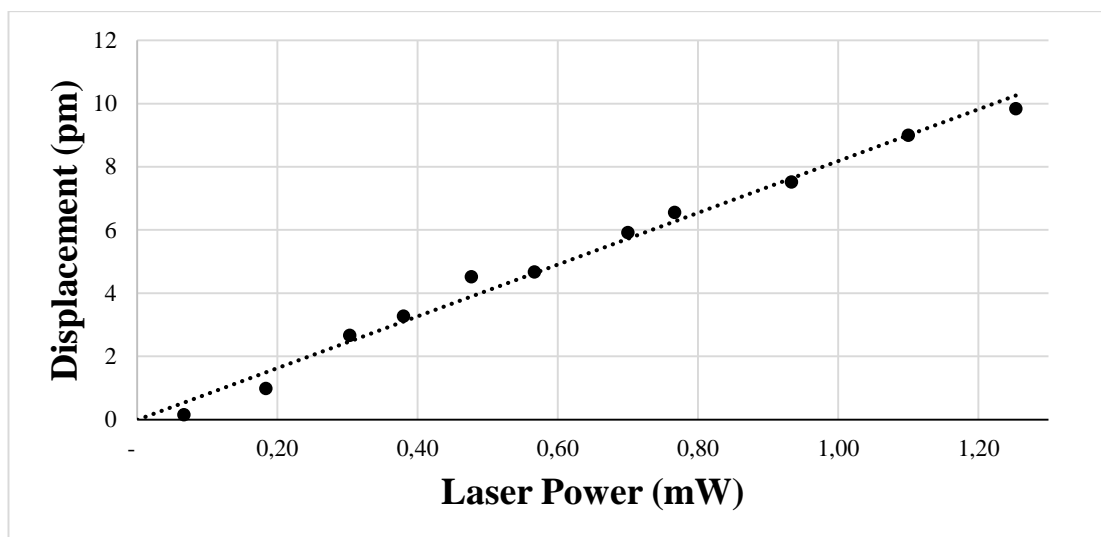

Figure 31: Displacement in pm is plotted against the excitation laser power with a linear fit. Output of the measurement interferometer is connected only to the Lock-In input.
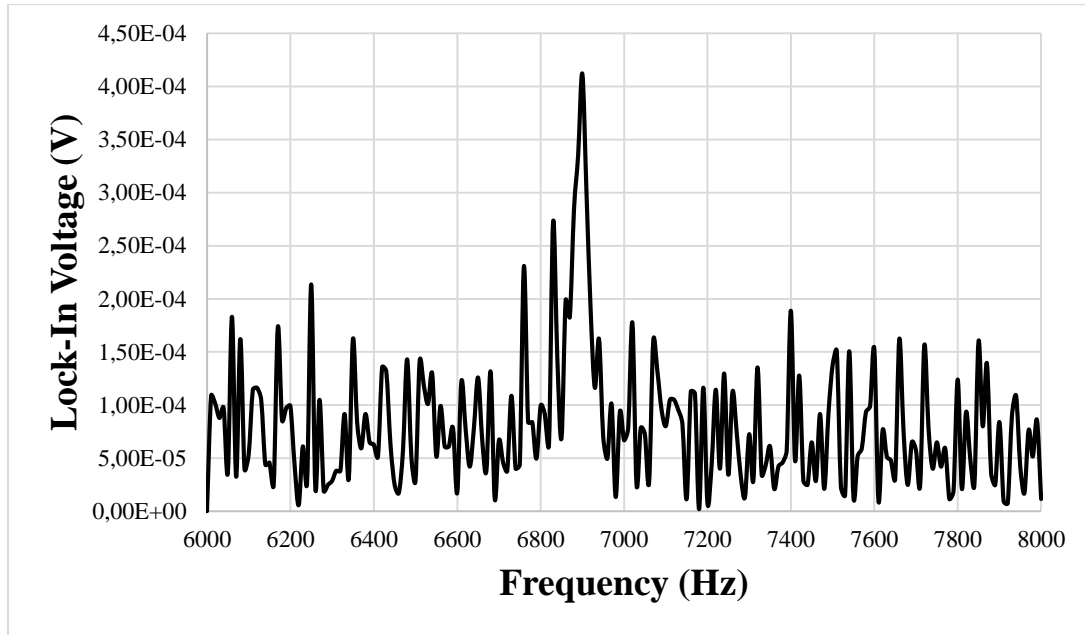
Figure 32: Lock-In data during laser excitation of the second fiber taken with 10 Hz resolution, $\tau = 1\ s$ and sensitivity set to $10\ mV$.

For the third fiber, the Lock-In data taken with piezo actuation can be seen in Figure 33. Lock-In times constant $\tau = 10\ ms$ and the sensitivity is set to $1\ V$ again for the piezo excitation measurements. The end face of the fiber is angled between $32 - 37°$. The calculated length from the microscope images indicate a length of $3.5\ \pm 0.2\ mm$ which means that the expected resonance frequency f_0 is between $7,399 - 9,301\ Hz$. The highest resonance peak for laser excitation is found to be at $8,965\ Hz$. The data taken is for $4\ mV$ excitation with $10\ Hz$ steps. The fiber before the final polishing process can be seen in Figure 34. For the laser excitation data, the Lock-In reserve is set to high reserve, sensitivity is set to $10\ mV$ and the time constant $\tau = 30\ s$. Displacement measured from the Lock-In amplifier can be seen in Figure 35 with the laser power for excitation modulated between $0 - 100\%$ using the software. The interference slope at the maximum data point is shown in Figure 36. The calculated quality factor $Q = 747$. Figure 37 shows Lock-In data taken during laser excitation of the fiber.
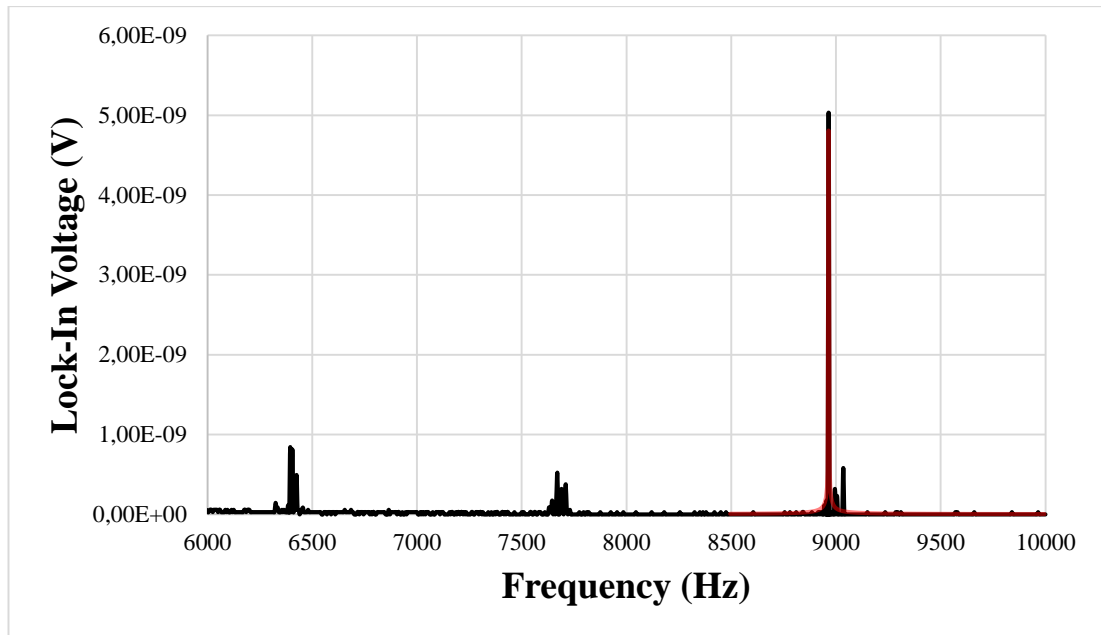
Figure 33: Amplitude data read from SR830 Lock-In Amplifier for piezo actuation of the second fiber with 4mV driving signal. The fit used for calculating the quality factor can be seen in red, $Q = 747$.

Figure 34: Close up of the third fiber used for taking measurements.

Figure 35: Displacement in pm is plotted against the excitation laser power with a linear fit. Output of the measurement interferometer is connected only to the Lock-In input.

Figure 36: Measurement interferometer slope for the data taken at the 100% excitation of the laser.

Figure 37: Lock-In data during laser excitation of the third fiber taken with $10\ Hz$ resolution, $\tau = 1\ s$ and sensitivity set to $10\ mV$.

CHAPTER V

RESULTS AND DISCUSSION

The displacement slopes read from the Lock-In amplifier in the previous section is for the total displacement measured for th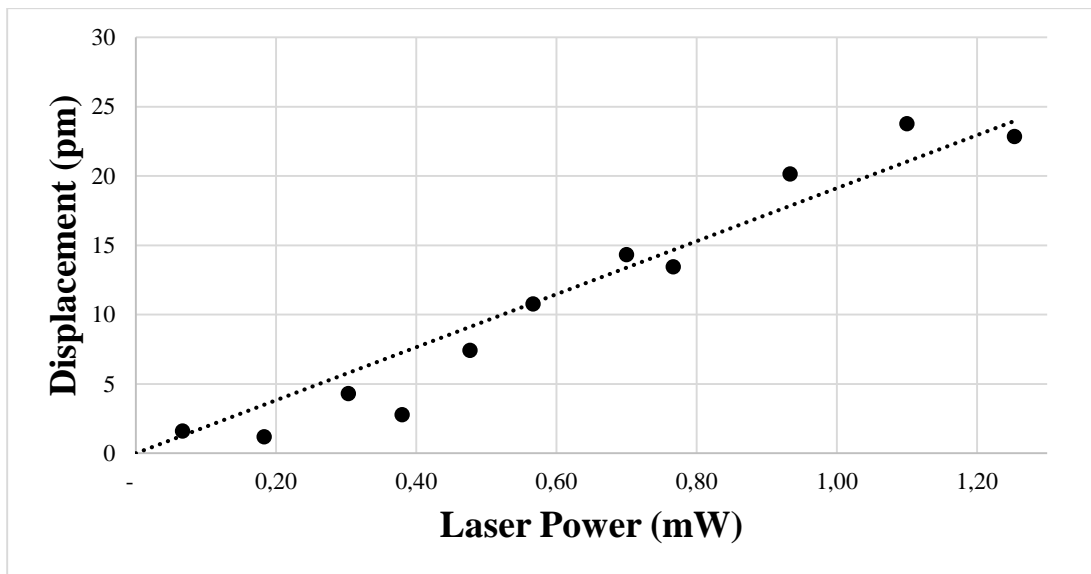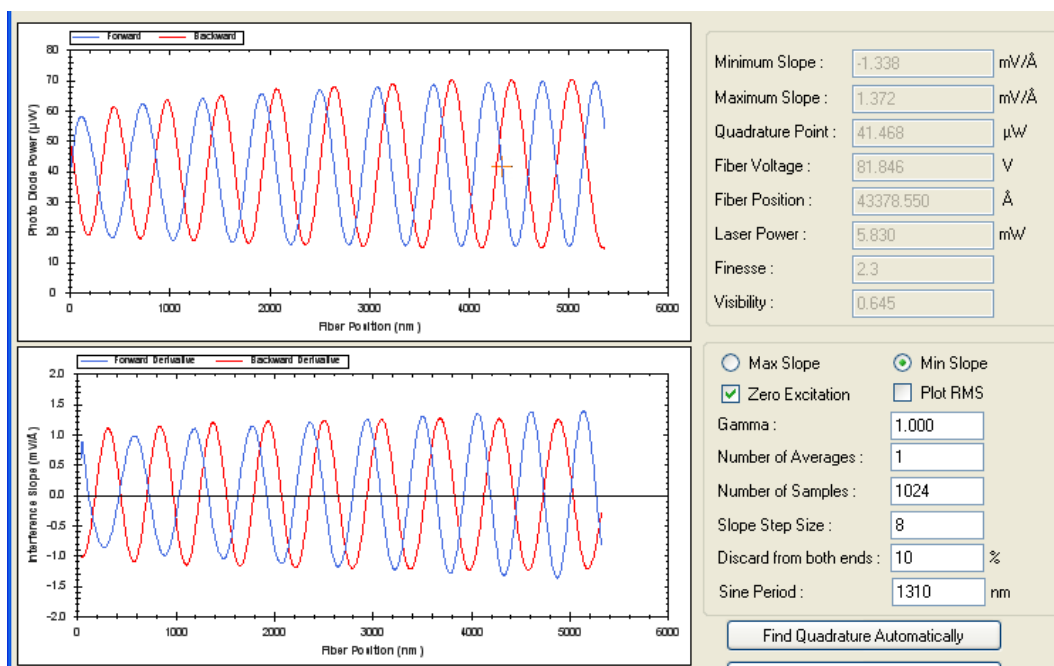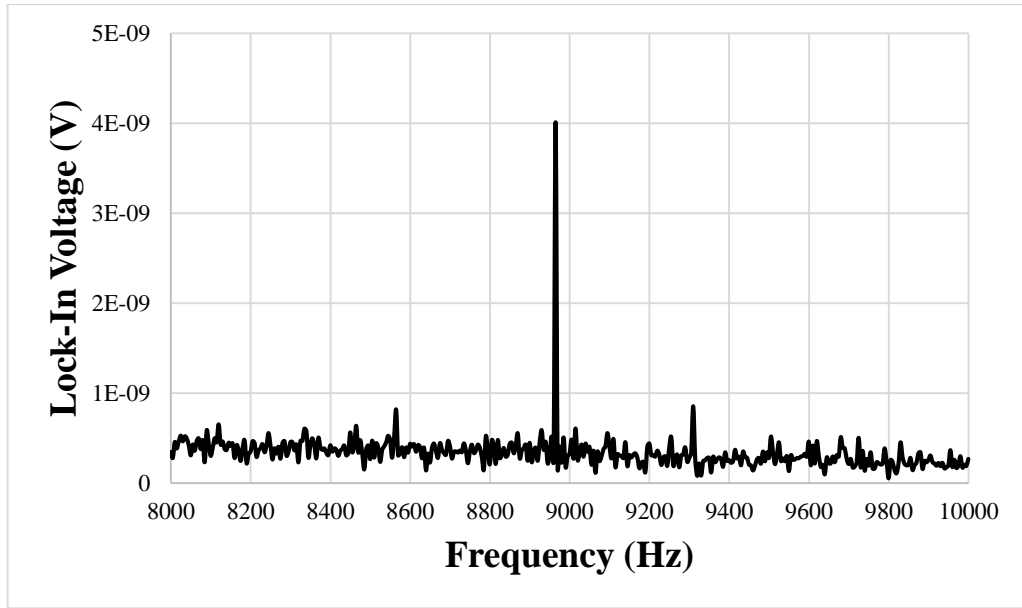e excited fibers for the total power delivered to the excitation fiber. As stated, there is a 2x2 coupler in the excitation interferometer which cuts the power delivered to the fiber in half. The excitation waveform is a square wave which has the amplitude of $2/\pi$ of the sine component for $1\ V$ of peak to peak signal at the excitation frequency. All the fiber measurements are taken a slight distance below from the tip to prevent any of the excitation signal from influencing the measurement interferometer, hence there is a small correction factor C that is applied to estimate the movement of the tip. The correction factors are calculated assuming small angle approximation for the total movement of tip of the fiber due to the fact that displacement at the tip is several orders of magnitude smaller than the total length of the fiber. Including the corrections, the measured slopes and the predicted displacement of the fiber for both Abraham and Minkowski theories are related by Eq.10.

$$m_{meas}C = Q_{meas}\Delta x_{calc}\frac{2}{\pi} \qquad \text{(Eq.10)}$$

The calculated values of displacement solely due to per mW of laser power without resonance for the Abraham and Minkowski cases are multiplied by the measured quality factor and plotted with the measured values and compared in Figures 38-40. The expected slopes including the errors in estimating the angle and the length of the fibers are shown in blue and red for the Minkowski and Abraham cases respectively

Figure 38: Expected displacement values resulting from the Abraham (red) and the Minkowski (blue) theory for the first fiber are shaded according to their error margins. The black line is from the measured value using the Lock-In with the shown linear fit.

Figure 39: Expected displacement values resulting from the Abraham (red) and the Minkowski (blue) theory for the second fiber are shaded according to their error margins. The black line is from the measured value using the Lock-In with the shown linear fit.
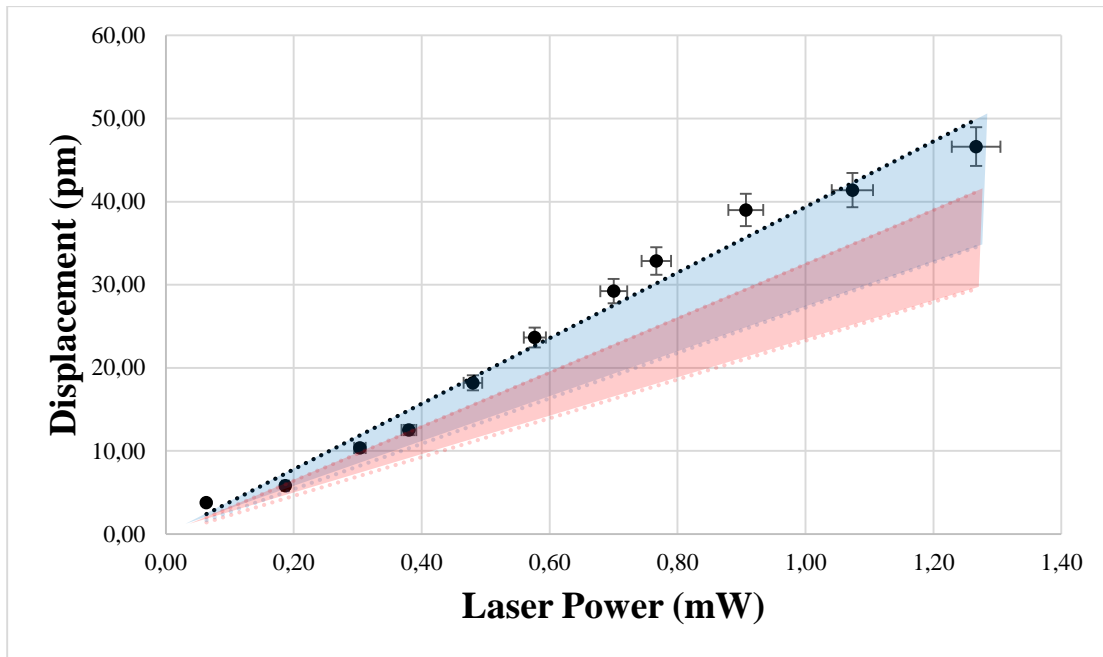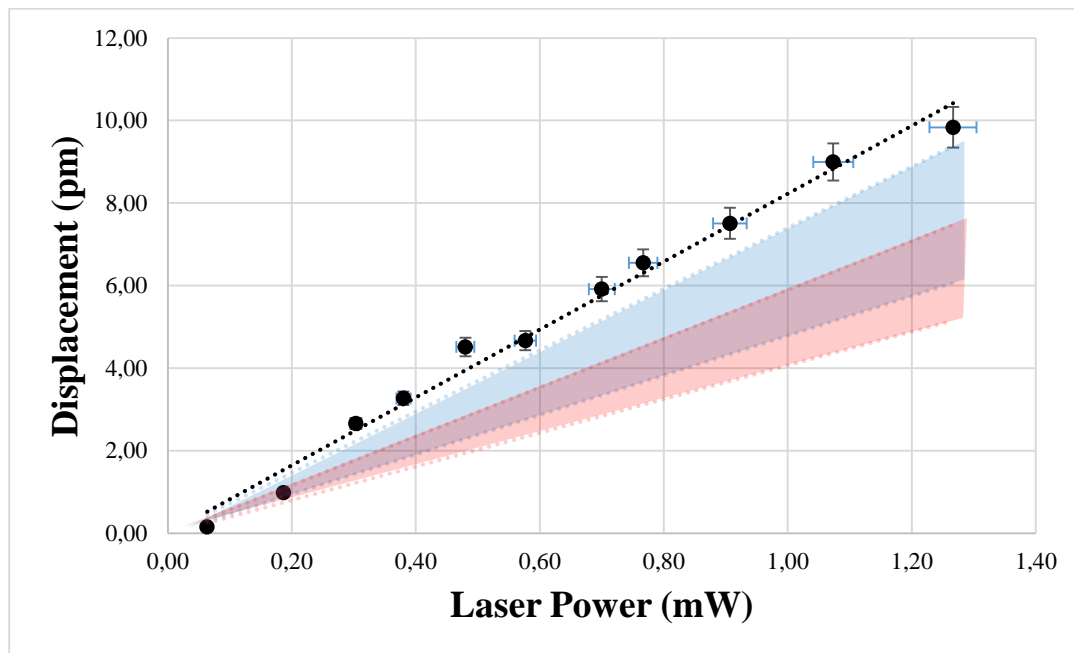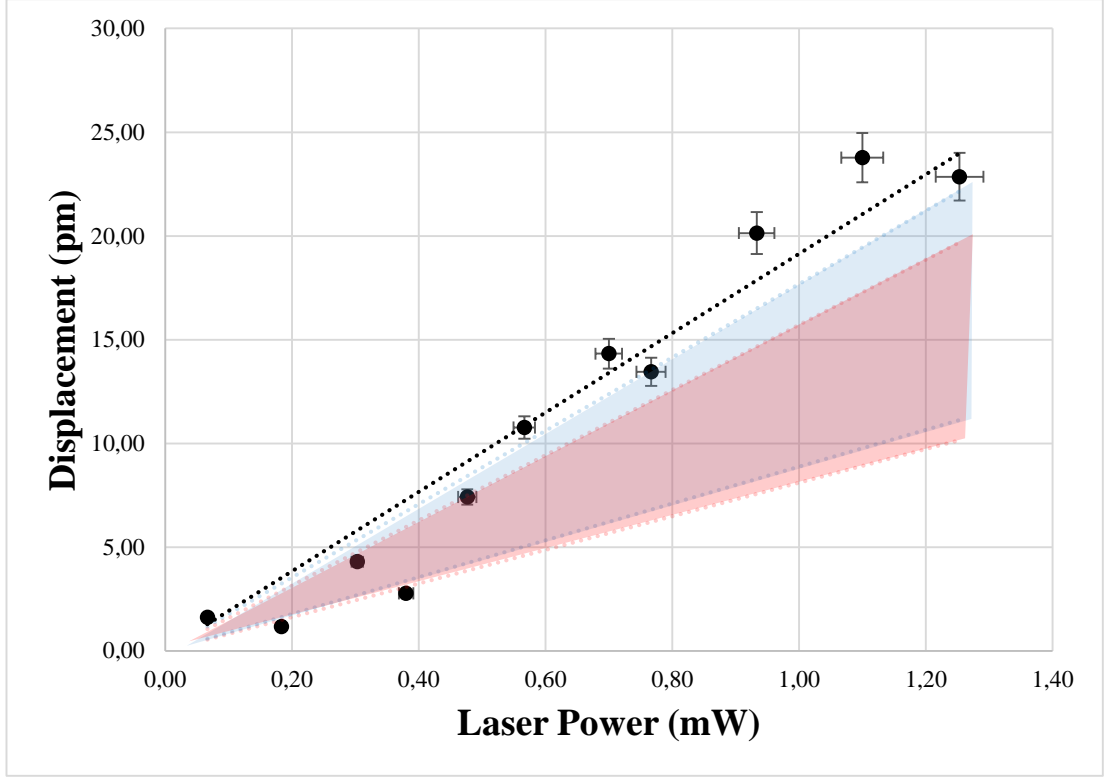
Figure 40: Expected displacement values resulting from the Abraham (red) and the Minkowski (blue) theory for the third fiber are shaded according to their error margins. The black line is from the measured value using the Lock-In with the shown linear fit.

The errors in the measurement data are primarily from possible angular mismatches in the alignment of the fibers. In case of perfect alignment, the direction of the measurement interferometer should be in the same plane as the cylindrical cross section of the excited fiber and the angled face should be in the same direction of the measurement interferometer. Tilts with respect to perfect alignment condition will change the measured displacement by a magnitude of $\cos \delta$. Assuming a maximum of 5° deviation for visual alignment, the total error in the measured data accounts to $\approx 2.4\%$. The laser photodiode used for the excitation has $\approx 0.03\ A/V$ uncertainty in its responsivity, which amounts to $\approx 3\%$ error in the power measurements. The data fitting is done with the requirement that the line passes through the origin. The dependence of the predicted force changes drastically depending on the end face angle of the excited fiber especially for angles above 35° which results in a wide margin of error even for small uncertainty in the angle measurements. However, the overall fits

45

are close and mostly within the values predicted by the Minkowski theory while differing more from the Abraham predictions.

The dominant contribution to the force in the calculations for the experimental setup at hand is due to the reflected light at the end face, which is physically the same system as a mirror inside a dielectric media. Considering the results obtained by Jones et al. [16,17] it is not surprising that the measurements are in favor of the Minkowski form since the experiments done on submerged mirrors consistently support the Minkowski theory. For similar experiments utilizing a mirror submerged in a dielectric medium, an argument is made by Kemp [14] that depending on whether the mirror is a perfect electrical conductor (PEC) or a perfect magnetic conductor (PMC), their calculations predict that only the Minkowski or Abraham form will be measurable respectively for such a system, hence does not necessarily rule out the possibility that the Abraham theory might appropriately describe some aspects of the momentum transfer exiting a silica filament as observed by She et al.

CHAPTER VI

CONCLUSION

The aim of this thesis was to measure the deflection caused on the tip of a fiber filament, angled at a certain degree in order to check which of the two rivaling forms for photon momentum in dielectric media would predict the outcomes most successfully. The results indicate that the Minkowski form of the photon momentum is more suitable in explaining the observed momentum transfer. Both the theoretical and the experimental evidence suggests, as pointed out by the proposed resolutions to the dilemma, that the rivaling forms do not constitute a complete picture by themselves without the addition of the appropriate material response. Experimental evidence of either form might contribute to a better theoretical understanding of the photon interactions between dielectric surfaces as well as provide an experimental insight for the design and improvement for applications utilizing radiation pressure such as solar sails, optical tweezers or optical cantilever excitation for Atomic Force Microscopy (AFM).

REFERENCES

[1] J. C. Maxwell, "A dynamical theory of the Electromagnetic field," *Philosophical Transactions of the Royal Society of London*, vol. 155, no. 0, pp. 459–512, Jan. 1865.

[2] "Gesammelte Werke. Band 8: Mysterium cosmographicum. Editio altera cum notis; de cometis; Hyperaspistes . Johannes Kepler," *Isis*, vol. 56, no. 4, pp. 478–479, Dec. 1965.

[3] W. She, J. Yu, and R. Feng, "Observation of a push force on the end face of a Nanometer silica filament exerted by outgoing light," *Physical Review Letters*, vol. 101, no. 24, Dec. 2008.

[4] P. Lebedew, "Untersuchungen über die Druckkräfte des Lichtes," *Annalen der Physik*, vol. 311, no. 11, pp. 433–458, 1901.

[5] E. F. Nichols and G. F. Hull, "Über Strahlungsdruck," *Annalen der Physik*, vol. 317, no. 10, pp. 225–263, 1903.

[6] H. Minkowski, "Die Grundgleichungen für die elektromagnetischen Vorgänge in bewegten Körpern," *Mathematische Annalen*, vol. 68, no. 4, pp. 472–525, Dec. 1910.

[7] M. Abraham, "Zur Elektrodynamik bewegter Körper," *Rendiconti del Circolo Matematico di Palermo*, vol. 28, no. 1, pp. 1–28, Dec. 1909.

[8] M. Abraham, "Sull'elettrodinamica di minkowski," *Rendiconti del Circolo Matematico di Palermo*, vol. 30, no. 1, pp. 33–46, Dec. 1910.

[9] N. L. Balazs, "The energy-momentum Tensor of the Electromagnetic field inside matter,"*Physical Review*, vol. 91, no. 2, pp. 408–411, Jul. 1953.

[10] C. Wang, "Plane wave in a moving medium and resolution of the Abraham-Minkowski debate by the special principle of relativity,". [Online]. Available: https://arxiv.org/vc/arxiv/papers/1106/1106.1163v75.pdf. Accessed: Sep. 6, 2016.

[11] On the Effect of the Motion of a Body upon the Velocity with which it is traversed by Light - Fizeau 1860

[12] M. J. Padgett, "On diffraction within a dielectric medium as an example of the Minkowski formulation of optical momentum," *Optics Express*, vol. 16, no. 25, p. 20864, Dec. 2008.

[13] S. M. Barnett, "Resolution of the Abraham-Minkowski dilemma," *Physical Review Letters*, vol. 104, no. 7, Feb. 2010.

[14] B. A. Kemp, "Resolution of the Abraham-Minkowski debate: Implications for the electromagnetic wave theory of light in matter," *Journal of Applied Physics*, vol. 109, no. 11, p. 111101, Jun. 2011.

[15] R. N. C. Pfeifer, T. A. Nieminen, N. R. Heckenberg, and H. Rubinsztein-Dunlop, "Colloquium: Momentum of an electromagnetic wave in dielectric media," Reviews of Modern Physics, vol. 79, no. 4, pp. 1197–1216, Oct. 2007.

[16] R. V. Jones, "Radiation pressure in a Refracting medium," *Nature*, vol. 167, no. 4246, pp. 439–440, Mar. 1951.

[17] R. V. Jones and B. Leslie, "The measurement of optical radiation pressure in Dispersive media,"*Proceedings of the Royal Society A: Mathematical, Physical and Engineering Sciences*, vol. 360, no. 1702, pp. 347–363, Apr. 1978.

[18] A. Ashkin and J. M. Dziedzic, "Radiation pressure on a free liquid surface," *Physical Review Letters*, vol. 30, no. 4, pp. 139–142, Jan. 1973.

[19] J. P. Gordon, "Radiation forces and Momenta in Dielectric media," *Physical Review A*, vol. 8, no. 1, pp. 14–21, Jul. 1973.

[20] N.-Y. Cui, "Surface deformation of a thin liquid film under infrared radiation," *Optics Communications*, vol. 308, pp. 85–90, Nov. 2013.

[21] A. F. Gibson, M. F. Kimmitt, A. O. Koohian, D. E. Evans, and G. F. D. Levy, "A study of radiation pressure in a refractive medium by the Photon drag effect," *Proceedings of the Royal Society A: Mathematical, Physical and Engineering Sciences*, vol. 370, no. 1742, pp. 303–311, Mar. 1980.

[22] M. Kristensen and J. P. Woerdman, "Is photon angular momentum conserved in a dielectric medium?," *Physical Review Letters*, vol. 72, no. 14, pp. 2171–2174, Apr. 1994.

[23] G. B. Walker and D. G. Lahoz, "Measurement of the Abraham Force in a barium titanate specimen," *Canadian Journal of Physics*, vol. 53, no. 23, pp. 2577–2586, Dec. 1975.

[24] I. Brevik, "Comment on 'Observation of a push force on the end face of a Nanometer silica filament exerted by outgoing Light'," *Physical Review Letters*, vol. 103, no. 21, Nov. 2009.

[25] M. Mansuripur, "Comment on 'Observation of a push force on the end face of a Nanometer silica filament exerted by outgoing Light'," *Physical Review Letters*, vol. 103, no. 1, Jul. 2009.

[26] M. Mansuripur and A. R. Zakharian, "Theoretical analysis of the force on the end face of a nanofilament exerted by an outgoing light pulse," *Physical Review A*, vol. 80, no. 2, Aug. 2009.

[27] V. P. Torchigin and A. V. Torchigin, "Comment on 'Theoretical analysis of the force on the end face of a nanofilament exerted by an outgoing light pulse'," *Physical Review A*, vol. 89, no. 5, May 2014.

[28] H. Choi, M. Park, D. S. Elliott, and K. Oh., "http://arxiv.org/abs/1601.05225," in *Optomechanical Measurement of the Abraham Force in an Adiabatic Liquid Core Optical Fiber Waveguide*. [Online]. Available: https://arxiv.org/ftp/arxiv/papers/1601/1601.05225.pdf. Accessed: Sep. 6, 2016.

[29] T. Ramos, G. F. Rubilar, and Y. N. Obukhov, "Relativistic analysis of the dielectric Einstein box: Abraham, Minkowski and total energy–momentum tensors," *Physics Letters A*, vol. 375, no. 16, pp. 1703–1709, Apr. 2011.

[30] R. V. Jones, "Some points in the design of optical levers and amplifiers," *Proceedings of the Physical Society. Section B*, vol. 64, no. 6, pp. 469–482, Jun. 1951.

[31] L. Tong *et al.*, "Subwavelength-diameter silica wires for low-loss optical wave guiding," *Nature*, vol. 426, no. 6968, pp. 816–819, Dec. 2003.

[32] [Online]. Available:
https://www.corning.com/media/worldwide/coc/documents/Fiber/SMF-28%20Ultra.pdf. Accessed: Sep. 6, 2016.

[33] [Online]. Available
http://www.thinksrs.com/downloads/PDFs/Manuals/SR830m.pdf. Accessed: Sep. 6, 2016.

Appendix A: MATLAB Code for Lock-In Control via RS232

```matlab
clear Freq Read Amp Phase
try
    fclose(instrfind);
end;
S = serial('COM##');
set(S, 'BaudRate', 9600, 'terminator', 13);
fopen(S);
TimeConst   = ##;
Sensitivity = ##;
SineAmp = ##;


StartFreq  = ##;
EndFreq    = ##;
Resolution = ##;
Freq  = [StartFreq:Resolution:EndFreq];
Read  = cell(1, length(Freq));
Amp   = zeros(1, length(Freq));
Phase = zeros(1, length(Freq));


%fprintf(S,'HARM 2');              %Harmonic detection


fprintf(S,'OUTX 0');              %RS232
fprintf(S,'FMOD 1');              %Internal oscillator
fprintf(S,'SLVL %f', SineAmp);    %Oscillator sine voltage
fprintf(S,'ISRC 0');              %Input A
fprintf(S,'IGND 0');              %Floating ground
fprintf(S,'ICPL 0');              %AC coupling
fprintf(S,'ILIN 3');              %Both notch filters
fprintf(S,'RMOD 0');              %High Reserve
fprintf(S,'SENS %f', Sensitivity); %Sensitivity
fprintf(S,'OFLT %f', TimeConst);  %Time constant
fprintf(S,'OFSL 3');              %Filter slope 24dB
fprintf(S,'SYNC 0');              % <200 Hz Sync filter off


for i = 1:length(Freq)
    fprintf(S,'FREQ %f\n',Freq(i));
    pause(##);
    fprintf(S,'SNAP?3,4'); Read{i} = fscanf(S,'%s\n');
end
fclose(S);


for j = 1:length(Read)
    for k = 1:length(Read{j})
        if Read{j}(k) == ','
            Amp(j) = str2double(Read{j}(1:k-1));
            Phase(j) = str2double(Read{j}(k+1:end));
            break
        end
    end
end
```